LA-13164-MS

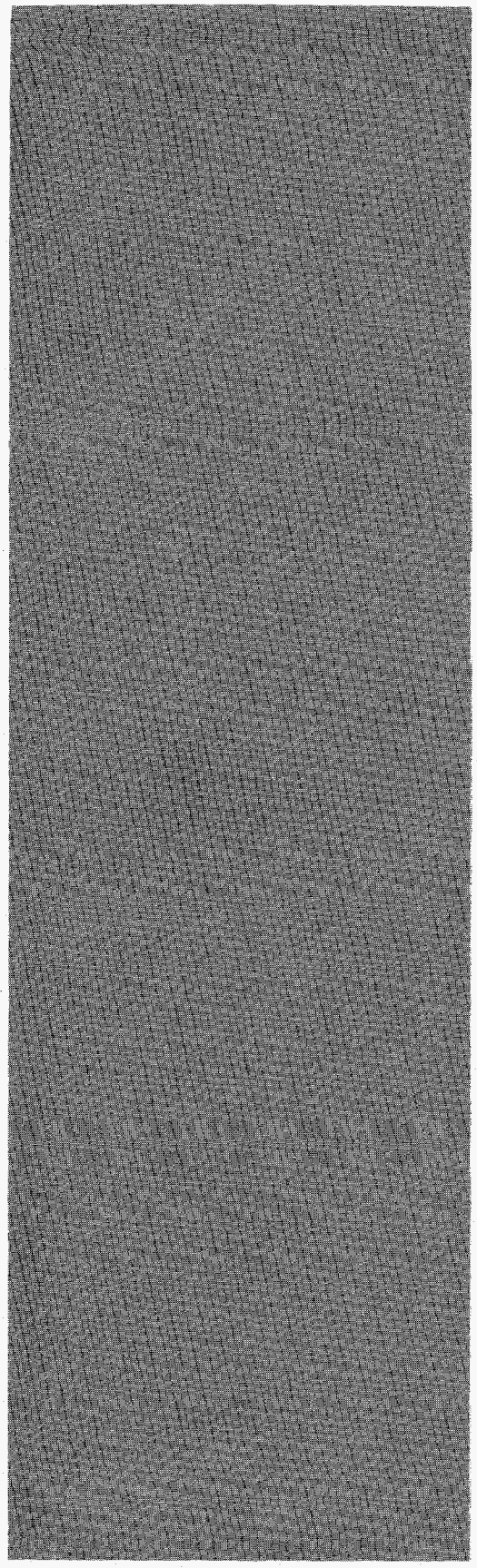

PBX 9501 High Explosive Violent Response/ Low Amplitude Insult Project: Phase I

Los Alamos
NATIONAL LABORATORY

Los Alamos National Laboratory is operated by the University of California for the United States Department of Energy under contract W-7405-ENG-36.

An Affirmative Action/Equal Opportunity Employer

LA-13164-MS
UC-741
Issued: January 1997

PBX 9501 High Explosive Violent Response/ Low Amplitude Insult Project: Phase I

D.J. Idar
R.A. Lucht
R. Scammon
J. Straight
C.B. Skidmore

Los Alamos
NATIONAL LABORATORY
Los Alamos, New Mexico 87545

TABLE OF CONTENTS

LIST OF TABLES

LIST OF FIGURES

PBX 9501 HIGH EXPLOSIVE VIOLENT RESPONSE/ LOW AMPLITUDE INSULT PROJECT: PHASE I

by

D. J. Idar, R. A. Lucht, R. Scammon, J. Straight, and C. B. Skidmore

ABSTRACT

Preliminary modeling and experimental analyses of the violent reaction threshold of semi-heavily confined PBX 9501 to low velocity impact have been completed. Experimental threshold measurements were obtained with ten tests using a spigot gun design to launch a hemispherical projectile at the high explosive contained in stainless steel. Powder curves were determined for several gun barrel designs, powders, and projectile materials and have proven to be very reproducible over the range of 75 to 325 ft/s. A threshold velocity of approximately 246 ft/s for violent reaction of the PBX 9501 was determined with experimental gauge and switch measurements and the remaining physical test evidence. Preliminary analyses of the PBX 9501 samples retrieved from both unreacted and partially reacted targets have been completed. Core samples were obtained from the unreacted targets and submitted for density determinations. The subsequent analysis supports the concept that the PBX 9501 yields and fractures under the low velocity compression event to expand and fill the annular gap in the target design. Samples of PBX 9501 from the partially reacted targets were examined with scanning electron microscope and light microscope techniques. Increased evidence of mechanical twinning effects are noted in the HMX crystals from the partially reacted targets. Finite element calculations using DYNA2D, with a modified ORION post processor, without reaction or chemistry models, were used to support the design of targets, to compare predictive analyses with experimental measurements, and to evaluate a proposed ignition criterion in a power law form for threshold to reaction with dependence on pressure, maximum shear strain rate, and time variables. The calculations show good agreement with the physical dent and deformation data from the remaining target evidence; however, they do not match the experimental pressure gauge measurements well. The differences can be attributed to a combination of the experimental variables, the need for better materials properties values in the calculations, and the need for chemistry and reaction in the predictions. Also, further evaluation of the ignition criterion form is needed to account for the probability of fracture in the PBX 9501.

I. INTRODUCTION

Strong shock-to-detonation-transition (SDT) of high explosives (HE) has been well characterized over several decades in shock wave physics research and finite element and hydrodynamic code analyses. These initiation mechanisms are normally associated with impacts of relatively high velocities, ≥ 1 mm/μs, and pressures, ≥ 10 kbars. More recently, the focus of energetic materials research has shifted to determining, defining, and predicting the phenomena associated with relatively weak, low amplitude insults and the probability for violent reaction leading to property damage and casualties.

These HE safety concerns are focused on the storage, handling, transport, and inadvertent initiation of conventional and nuclear weapons, and methods related to disposal, dismantlement, and replacement. Examples of these events include the impact experienced by a weapon if it is accidentally dropped, or the collision of a projectile with a weapon in storage or transport. Under these conditions the potential exists to either sensitize the HE or to produce a violent reaction with a possible loss of life and property. The goal is to identify the relevant parameters: mechanical, chemical, confinement, and impact conditions that lead to sensitization, initiation, and/or violent reaction of the HE. This knowledge will assist in the development and verification of our predictive code capabilities. This knowledge will be used to establish and modify those methods associated with the safety issues.

PBX 9501, a LANL formulation, was chosen for our research because it represents a large portion of the HE in the remaining nuclear stockpile. It is a 95.0/2.5/2.5 wt % HMX/Estane/BDNPA-BDNPF formulation[1] with a theoretical maximum density (TMD) of 1.860 g/cm^3 and a nominal detonation velocity of 8.83 mm/μsec. The average density of the samples used for the research reported here was 1.837 g/cm^3 (~98.7% TMD).

The LLNL DYNA2D finite element code was chosen to support the modeling effort. This included experiment design calculations, material model development, and analysis of the experimental results. This code was also used to investigate the PBX 9501 ignition criterion developed by Richard Browning.

II. BACKGROUND

Recently Steven Chidester et al.[2] reported on their experimental and theoretical DYNA2D analyses of low pressure impacts on the explosives LX-10-1 and LX-17-0. Their methodology, based on frictional work for ignition, was used to predict the projectile threshold velocity to produce a violent event in the LX-10-1. However, they were unable to obtain a reaction in the LX-17 under their experimental conditions.

The explosive LX-10-1 is a LLNL formulation with 94.5/5.5 wt % HMX/Viton A[3] with a TMD of 1.895 g/cm^3 and a nominal detonation velocity of 8.85 mm/μs. The critical temperatures of LX-10-1 and PBX 9501 are essentially the same, 215°C, and the drop weight impact heights differ little. However, they do differ in their skid, Susan, and spigot test (a different test than described in this report) results, with LX-10-1 showing more sensitivity. For their research, Chidester and coworkers used LX-10-1 samples with an average density of 1.86 g/cm^3 (≈98.2% TMD).

The explosive LX-17-0 is also a LLNL formulation with 92.5/7.5 wt % TATB/Kel-F 800 with a TMD of

1.944 g/cm^3 and a nominal detonation velocity of 7.63 mm/μs. The average density of their samples was 1.90 g/cm^3 (~97.7% TMD).

For their impact tests, Chidester et. al. employed a 2.56 kg, hemispherical nose, tantalum (Ta) projectile with a 0.46 kg sabot launched from a smooth bore 76-mm diam. gas gun at a LX-10-1, metal encased, plane geometry target. They measured v_{50} values for this arrangement ranging from ~106.0–115.8 ft/s (32.3–35.3 m/s), which produced explosions. For comparison, a velocity of 1750 ft/s (533 m/s) is required to produce an SDT 0.5-in. run-to-detonation in PBX 9501 with a flat, mild steel plate impact based on 1-D Hugoniot[3] matching calculations and the PBX 9501 Pop plot. Significantly higher velocities would be required for SDT driven by a hemispherical impactor because the shock waves produced would be highly divergent. Similar tests by Chidester et. al. on LX-17-0 encased targets and with a projectile velocity as high as 463.3 ft/s (141.2 m/s) did not produce a violent reaction.

III. EXPERIMENTAL

A. Spigot Gun, Projectile Description, and Powder Curve Tests

The projectile characteristics required by this project were a 2 kg projectile of arbitrary size and shape traveling at velocities from 75 ft/s to 325 ft/s (≈22 to 100 m/s). The arbitrary size and shape limited the utility of a conventional projectile-in-tube launch system, which would have required an elaborate sabot design and a massive sabot stripper. Although a gas driven system would have worked well for the 75 ft/s, it would have had trouble achieving the 325 ft/s needed.

For these reasons, a powder gun driving a spigot projectile was designed with the use of either BLC2 or IMR 4350 rifle powder. A small bore diameter was needed to burn the gunpowder reliably at high pressures. A small bore diameter and short barrel were also needed to achieve the very low 75 ft/s. The initial design had a 0.5-in. diam. bore with a 9-in. long barrel. For simplicity, a rimmed rifle cartridge (.45-70 cal.) is used. A 1.5-in. long polyethylene obturator is used to seal the powder gas products. The projectile has a head of arbitrary size and shape driven by a 0.5-in. diam. by 5.25-in. long shank (spigot). The current projectile has a 3-in. diam. hemispherical nose, is made of cold rolled mild steel, and has a total mass (with spigot) of 2 kg. The gases are vented before the projectile leaves the bore to reduce tip-off. This gun worked well at low velocities, but the spigot buckled in-bore at higher velocities. Thus, the design was modified to a 0.75-in. bore still using the 0.45-70 cal cartridge. The new barrel has a 2-in. OD and is made of mild steel. The receiver or breech block has a 4-in. OD and is also made of mild steel. The barrel screws into the breech block with an Acme thread.

Because the projectile is so massive (compared to normal rifle bullets), the powder burns almost as if it was in a closed container. As such, the burn characteristics do not match any published data, and computer code predictions are of little value. Thus, we have made some attempts to measure the burn pressure using piezoelectric pressure transducers. We have consistently overranged the 100,000 psi (~689 MPa) transducers and have, on several occasions, literally blown them out the side of the barrels. We hope to pursue these pressure measurements next year. Even with the 0.75-in. diam. spigot, we see plastic deformation of the base of the spigot at velocities above ~250 ft/s. We have achieved over 300 ft/s using hardened spigots. In an attempt to reach 330 ft/s, we ruptured a barrel. Higher velocities required a thicker, higher strength barrel. At this time, the powder weight vs. velocity curve for the 2-in. barrel is well established, and the gun is performing reliably. A total of 71 tests has been fired with the 0.75-in. bore gun. Different barrels have slightly different powder curves due to small manufacturing variances.

A higher pressure barrel has been designed and fabricated, and initial testing has been completed. The

barrel has a 3-in. OD, is made of AISI 4340 steel heat treated to Rockwell hardness range "c" (Rc) 35, and uses a 0.45-basic cartridge. The breech block has a 6-in. OD. The 0.45-basic cartridge is about 1 in. longer than the 0.47-70 that we use with the 2-in. barrel. The extra length has two effects. The first, of course, is to allow us to use more powder. The second effect is that we have more ullage and, thus, a significant shift in the powder weight vs. velocity curve. Because we are operating at extremely high pressures, we are using strain gauges to measure the pressure history. Hoop and axial strain gauges are mounted on the barrel over the chamber. An example of the strain measurement is shown in Figure 1. The two measurements can be combined to compute the bore pressure as a function of time. This is shown in Figure 2. The peak pressure in this test was 154,000 psi (~1.07 GPa). A gun barrel is neither a closed cylinder nor an open one. One might expect the axial strain to lie between these two conditions (tensile and a fixed fraction of the hoop strain). As can be seen in Figure 1, the axial strain clearly does not conform to these expectations. The strain starts out negative (compressive) and then oscillates with a high amplitude. The initial compression is due to the Poisson effect combined with the undefined end conditions. The initial local contraction of the material then excites the fundamental mode of axial vibration, and the barrel begins to oscillate. This explanation was verified by comparing a Fast-Fourier-Transform (FFT) of the axial strain gauge data with a finite element analysis of the entire gun assembly. All of the FFT analyses show a strong peak at 2 kHz, which correlates with the fundamental mode of vibration from the finite element analysis.

We have completed a total of 12 tests with the high pressure gun. Of these, 6 included strain gauges; however, data were collected on only three because of recording difficulties. One of the tests was the highest velocity possible and at a live target. We achieved 325 ± 5 ft/s.

Because of the short barrels on all of these guns, a relatively flexible gun mount, and the very forceful recoil, the projectile hit point varies considerably from test to test. It is often up to 1-in. high in 6 ft of flight, and varies from 1-in. left to 1-in. right of the aim point. To achieve better hit accuracy, later tests were performed by moving the gun to within 4 ft of the target. Targets that reacted violently usually damaged the barrel.

For safety reasons, no arming energy is permitted on the firing mound until all personnel are safely inside

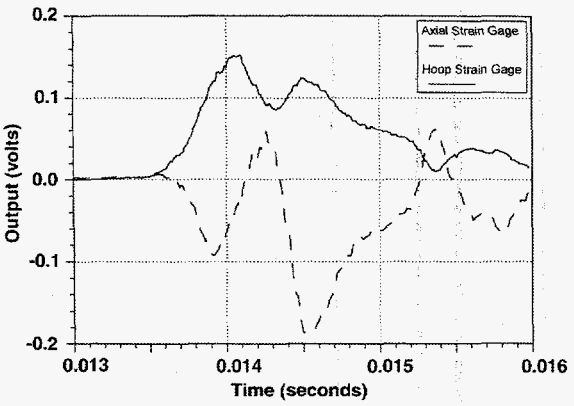

Figure 1: Hoop and axial strain measurements obtained from the high pressure barrel design for the spigot gun.

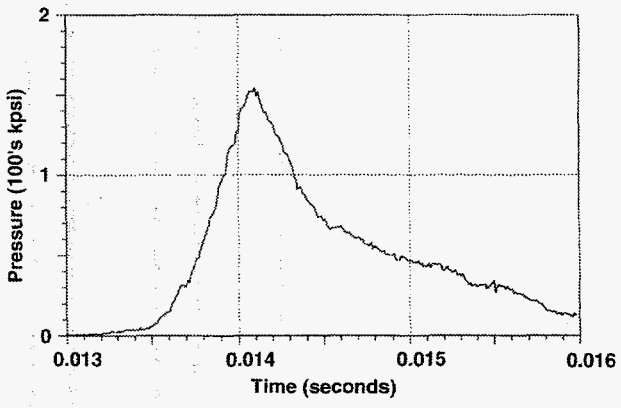

Figure 2: Bore pressure as a function of time for the high pressure barrel design.

the bunker. Thus, an electrically actuated, pneumatically driven firing mechanism was designed. The final electrical and compressed air connections are made from inside the bunker after the area is cleared.

One of the most important performance characteristics of the gun is the projectile velocity. Because most of the powder gases are vented before the spigot leaves the muzzle, a velocity measurement can be made very close to the muzzle. Because of the proximity of the gun to the target, any instrumentation on the gun, target, or between the two would be vulnerable to target detonation. An inexpensive, easily replaceable light/photodiode system was designed by Bob Critchfield to determine the projectile velocity. It is composed of three sets of halogen lights and photodiodes spaced at 3-in. intervals in a wooden frame. The photodiode outputs are recorded on digital oscilloscopes. The three profiles yield two independent velocity measurements. An average velocity was then determined from these two values, and this value is reported with the powder curve results and the live target test results. A photograph of the spigot gun with a light/photodiode system is shown in Figure 3, and the performance data are given in Tables 1 and 2.

B. Inert Target Description

The inert targets were built with multiple layers of 0.5 to 1.0-in. thick plywood sandwiched together with staples or nails. The inert targets were used to verify aiming for the gun, to establish the powder curve, and to test the triggering mechanisms for the diagnostics. Crosshairs were drawn on the targets to determine the impact accuracy.

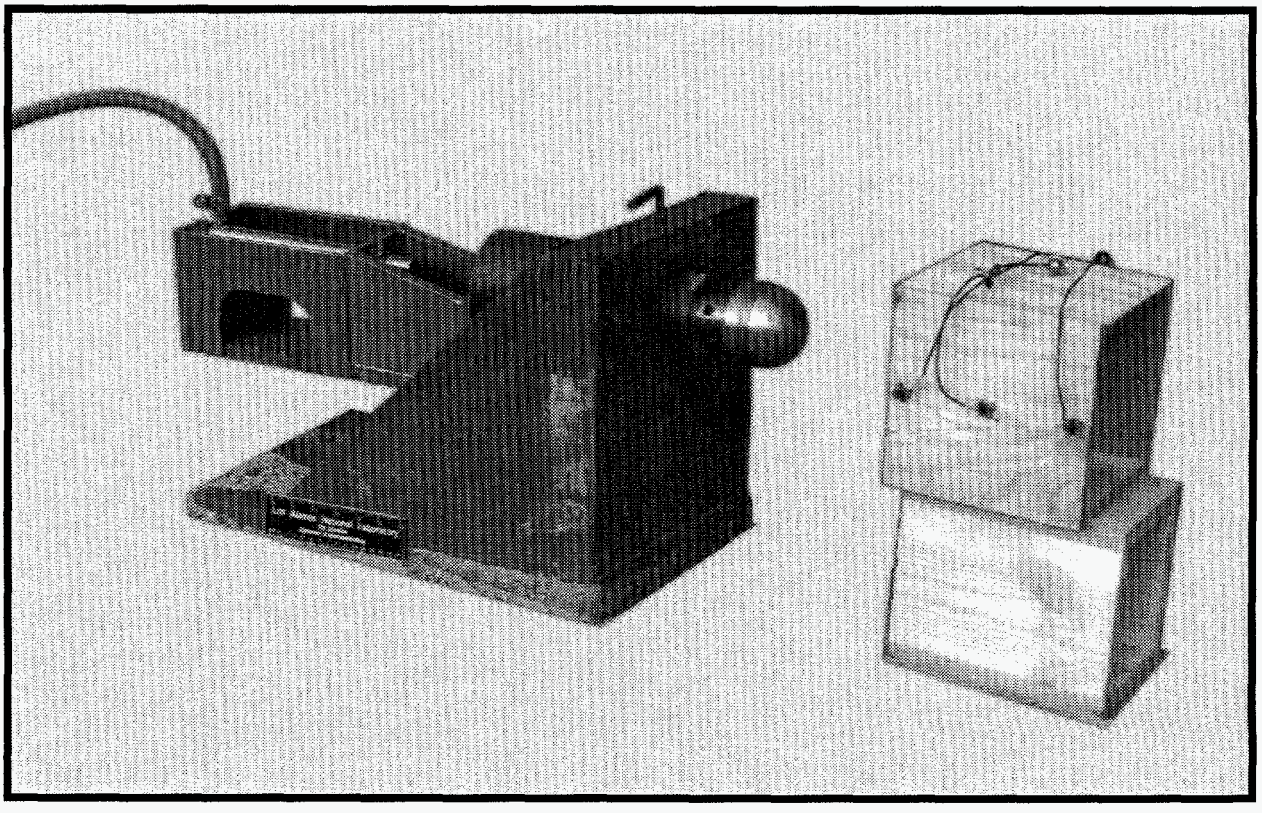

Figure 3: Spigot gun and photodiode velocity screen box.

Table 1. Powder curve performance results for low pressure barrel design (BLC2).

TEST #	Powder Wt. (g)	Velocity (ft/s)	Comments
DF15-548	2.0	104.038	old obturator
DF15-549	2.5	115.989	
12/14/94	2.75	no velocity data	primer burned only, below freezing temp.
12/14/94	2.75	no velocity data	primer burned only, below freezing temp.
12/14/94	2.75	no velocity data	primer burned only, below freezing temp.
DF15-550	3.0	152.932	
DF15-581	3.0	184.68	
DF15-551	3.5	208.15	
DF15-582	3.5	205.281	
DF15-583	3.5	231.84	new obturator
DF15-2364	3.5	234.95	impact 1-in. high, new obturator
DF15-584	4.0	240.493	
DF15-552	4.0	227.025	
DF15-2365	4.0	256.00	estimated impact 1-in. high
DF15-2366	4.0	255.31	impact 1-in. high, new obturator
DF15-587	4.001	236.748	
DF15-2350	4.5	269.01	impact 1.25-in. high, new obturator
DF15-2351	4.5	265.726	impact 0.75-in. high, new obturator
DF15-585	4.5	no velocity data	transducer blowout
DF15-642	4.507	256.714	
DF15-586	5.0	no velocity data	transducer blowout
DF15-644	5.0	264.575	new barrel, new obturator
DF15-803	5.0	no velocity data	new barrel
DF15-643	5.003	no velocity data	old obturator- transducer blowout
DF15-2345	5.261	264.84	impact 1-in. high, new obturator
DF15-2346	5.261	no velocity data	impact 1.25-in. high, new obturator
DF15-2347	5.261	264.939	new obturator
DF15-2318	5.261	269.266	impact 1.5-in. high
DF15-2319	5.261	278.589	
DF15-2317	5.262	267.241	impact 1.5-in. high
DF15-2376	5.325	308.8	impact 0.5-in. high, 1.0-in. left, new obturator
DF15-2377	5.325	310.4	impact 0.5 -in. high, 1.0-in. left, new obturator
DF15-665	5.425	no velocity data	barrel blowout
DF15-2384	5.44	no velocity data	barrel blowout

Table 1. Powder curve performance results for low pressure barrel design (IMR4350).

Test #	Powder Wt. (g)	Velocity (ft/s)	Comments
DF15-2326	1.25	95.222	impact 0.5-in. high, old obturator
DF15-2327	1.25 + cow	128.275	impact 0.5-in. right, 0.25-in. high, new obturator, cow ≡ excess case volume was filled with cream of wheat
DF15-2323	2.75	189.998	impact on crosshairs, old obturator
DF15-2324	2.75	188.868	impact 0.5-in. high, old obtrurator
DF15-2325	2.75	185.556	impact 1-in. high, old obturator
DF15-2328	3.25	no velocity data	impact 1-in. high, new obturator
DF15-2329	3.25	218.521	impact 1-in. high,0.5-in. left, new obturator
	3.25	214.94	impact 0.375-in. high, 0.375-in. left
DF15-2367	3.4	234.9	impact 1-in. high, new obturator
DF15-2368	3.4	232.6	impact 0.5-in. high, new obtrurator
DF-2358	3.5	no velocity data	impact 1-in. high, new obturator
DF-2359	3.5	237.91	impact 1-in. high, 0.75-in. left, new obturator
DF-2364	3.5	234.95	impact 1-in. high, new obturator
K3-1238	3.6	244.5	impact 0.5-in. low, 1- in.right
K3-1277	3.6	241.75	0.5-in. low, 5-in. left [1]
K3-1278	3.6	236.96	0.5-in. high, 0.125-in. left [1]
K3-1286	3.7	243.996	[1]
K3-1287	3.7	245.151	[1]
K3-1290	3.7	246.345	target exploded, barrel destroyed
K3-1136	3.8	255.95	impact 1-in. left [1]
K3-1237	3.8	251.85	impact 0.5-in. high, 1-in. left [1]
DF15-2401	3.9	252.525	impact 0.875-in. high, 1.25-in. left
DF15-2402	3.9	250.627	impact 1.25-in. high, 0.875-in. left
K3-1135	3.9	no velocity data	impact 1.5-in. high
K3-1140	3.9	no velocity data	impact 0.75-in. high
K3-1174	3.9	251.256	impact on crosshairs
K3-1182	3.9	252.8	impact 0.5-in. high, 1.5-in. left [1]
K3-1183	3.9	242.7	impact 0.5-in high, 0.25-in left, spiked tip projectile

[1] Optical sight was adjusted between tests, thus the hit point data is of little significance.

Table 1. Powder curve performance results for low pressure barrel design (IMR4350 cont.).

Test #	Powder Wt. (g)	Velocity (ft/s)	Comments
K3-1233	3.9	248.76	impact 0.25-in. high, 0.25-in. left, spiked tip projectile
K3-1234	3.9	246.3	impact on crosshairs, spiked tip projectile
K3-1235	3.9	no velocity data	target exploded, barrel destroyed [1]
DF15-2360	4.0	252.57	impact 1-in. high, new obturator
DF15-2361	4.0	249.23	impact 1-in. high, new obturator
DF15-2382	4.0	256.7	impact 0.5-in. high, 1-in. right, new obturator
DF15-2383	4.0	253.9	impact 0.75-in. high, 1.0 in left, new obturator
DF15-2362	4.5	274.65	impact 1-in. high, new obturator
DF15-2363	4.5	271.48	impact 1.25-in. high, new obturator

[1] Optical sight was adjusted between tests, thus the hit point data is of little significance.

C. Live Target I Description

The original target design was based on a modification of the target assembly used by Chidester et. al.[2] with the following modification: ten target assemblies have been machined from 304 ss according to the scales and dimensions given in Clinton Shonrock's drawing number 139Y-600005,[4] consisting of a holder, disc, and retaining ring. Both the holder and retaining ring are machined with eight evenly dispersed holes to allow for assembly of the target. The PBX 9501 and Sylgard 184 potting articles were also manufactured according to the same drawing descriptions, with diameters of 5.75-in. each, and thicknesses of 1.00-in. and 0.020-in, respectively. The stainless steel cover disc was nominally 0.125 ± 0.001-in. thick with a flatness of 0.002-in. across the 5.75-in. diam. Densities were determined for each of the PBX 9501 articles, with an average density of 1.837 g/cm^3. The density information for each HE article is provided in Table 3. Assembly of the targets was performed by ESA personnel at TA-16, Bldg. 410, according to the assembly procedures written by either Ron Flury or Dick Scammon. The original design dimensions allowed for an annular gap of 0.125-in. between the HE O.D. and the holder I.D. Figure 4 is a schematic of the target design I. Seven 1/2-13 hex nuts and bolts are used to secure the holder, the PBX 9501 piece, the Sylgard 184, the disc cover, and the retaining ring together. The eighth hole is used to secure the assembly to the mild steel backing plate described below. Four assemblies, targets 1–4, were assembled in this fashion and used for the first four spigot gun tests.

Table 2: Powder curve performance results for high pressure barrel design (IMR4350).

Test #	Powder Wt. (g)	Velocity (ft/sec)	Comments
K3-1288	3.5	no velocity data	impact 1.5-in. high[1]
K3-1289	4.0	241.26	impact 1.5-in. high[1]
K3-1336	4.5	252.8	impact 1.5-in. high[1]
K3-1337	5.0	271.0	impact 1.5-in. high[1]
K3-1339	5.0 + cow	291.7	impact 0.25-in. high, 1.0-in. left, cow ≡ excess case volume was filled with cream of wheat [1]
K3-1338	5.5 + cow	285.47	[1]
K3-1340	5.5 + cow	302.4	impact 1.0-in. high[1]
K3-1341	6.0	282.9	[1]
K3-1342	6.5	319.8	141,200 psi chamber pressure [1]
K3-1343	7.0	no velocity data	152,500 psi chamber pressure [1]
K3-1344	7.0	325.75	154,000 psi chamber pressure [1]
K3-1304	7.0	no velocity data	(1)

[1] Optical sight was adjusted between tests, thus the hit point data is of little significance.

Table 3: PBX 9501, lot number HOL96C73 1, density report. All measurements were determined at 73.00°F.

Piece Number	Dry Wt. (g)	Wet Wt. (g)	Volume (cm^3)	Density (g/cm^3)
45614-0001	780.10	356.20	424.923	1.836
45614-0002	780.30	356.50	424.823	1.837
45614-0003	780.50	356.70	424.823	1.837
45614-0004	780.30	356.30	425.023	1.836
45614-0005	780.70	356.60	425.123	1.836
45614-0006	780.90	356.80	425.123	1.837
45614-0007	780.70	356.30	424.422	1.837
45614-0008	780.50	356.70	424.823	1.837
45614-0009	780.10	356.50	424.622	1.837
45614-0010	780.20	356.30	424.923	1.836

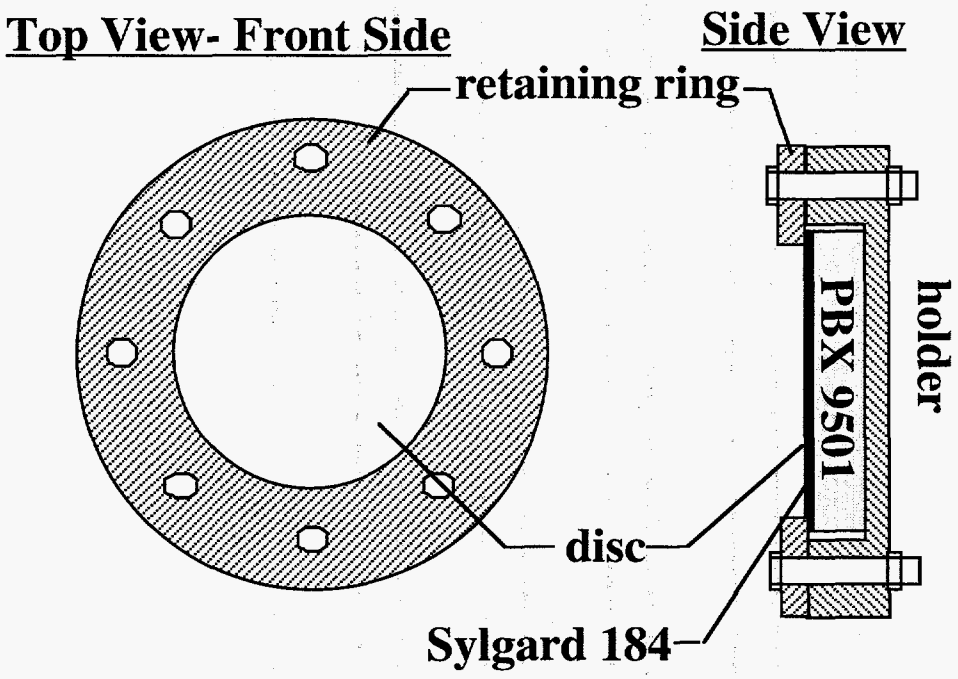

Figure 4: Live target design I. The PBX 9501 is 5.75-in. in diameter, and 1.00-in. thick.

D. Mild Steel Backing Plate Description

A 12.0-in. square, 3.0-in. thick piece of mild steel was machined to serve as a high impedance backing plate for the target assembly. A 0.25-in. deep, ~6.0-in. diam. circle was milled into the center of the steel backing plate to allow for target rear surface deformation. Seven holes were countersunk into the plate to accommodate the seven assembly nuts and bolts on the target. An eighth hole was drilled through the backing plate to use a nut and bolt to secure the target to the backing plate.

E. Live Target II Description

Modifications were made to the target holder, the assembly procedure, and the mild steel backing plate for gauge diagnostics on targets 5 and 6. Figure 5 depicts the target assembly with the new diagnostics. The new diagnostics included one Dynasen ≈50Ω carbon film gauge, five Dynasen ≈50Ω pinducers, and eighteen foil switches. The foil switches (based on Ken Uher's design), located on the front surface of the target, were used to determine the position and timing of the projectile impact. Nine foil switches were positioned parallel with the vertical axis of the target, and the remaining nine were positioned perpendicular to this axis. They were spaced with centers separated by 0.5-in. starting on the target center. The purpose of the carbon film gauge was to measure pressures produced by the compression event and any subsequent reaction. The gauge element was positioned over the center of the PBX 9501 piece and potted in the Sylgard 184 layer. The purpose of the pinducers was to measure the low pressure produced in the HE at the time of impact and longer if possible. For a description of, and a calibration procedure for the pinducers see Roy Lucht and Jacque Charest's[5] recent APS paper. Three pinducers were positioned flush with the back, inside surface of the stainless steel (ss) holder during the assembly process: one on center,

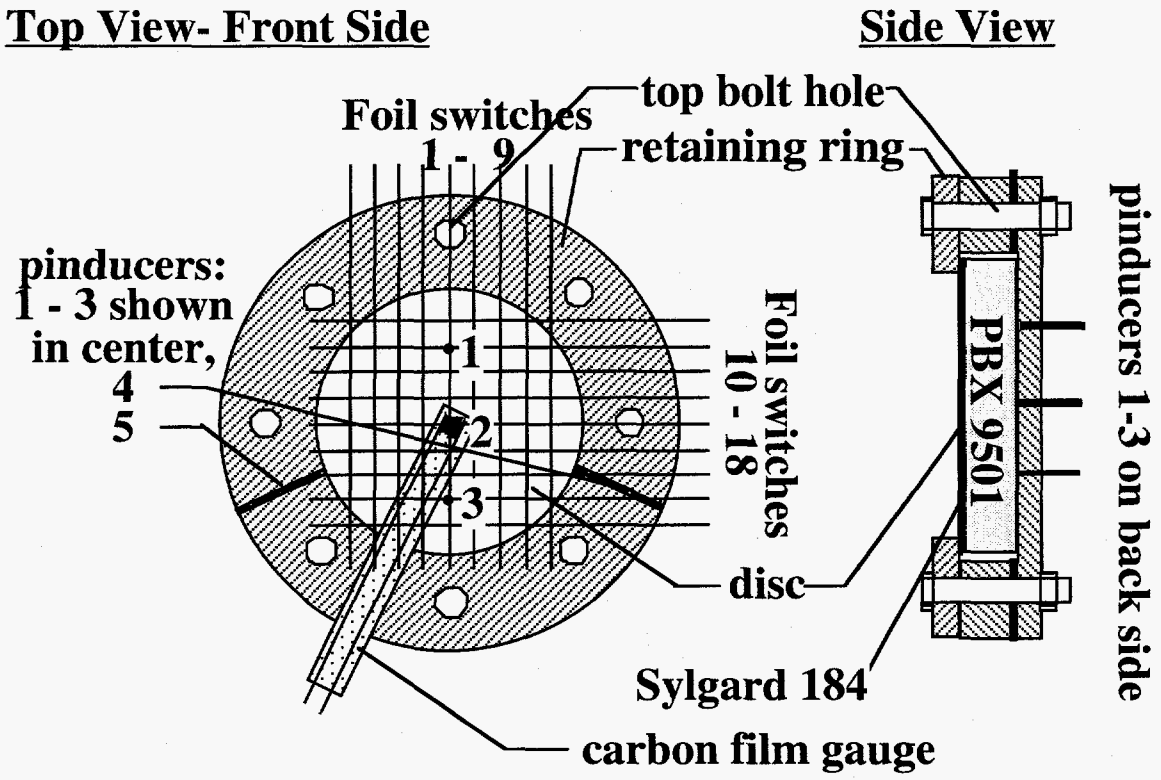

Figure 5: Live target design II, with 18 foil switches, one carbon film gauge, and 5 pinducers.

and one each 1.5-in. off the vertical center. The two additional pinducers were positioned radially with the gauge element flush to the inside surface of the ss holder, near the back surface of the PBX 9501 cylinder. One of the purposes of the radial pinducer was to measure the time at which the HE came into contact with the side wall of the holder. All of the pinducers were secured in position with epoxy in this target design. The mild steel backing plate was drilled with three additional holes to allow for the pinducers and cable connections on the back side of the target holder.

F. Live Target III Description

Further modifications were made to targets 7, 8, 9, and 10, the assembly procedure, and the mild steel backing plate to add two more pinducers and a thermocouple to the design, to change the location of the two radial pinducers, and to reduce the number of foil switches from eighteen to fourteen. Figure 6 shows the new pinducer, foil switches, and carbon film gauge locations.

The two additional pinducers were added to the back side of the target, 1.5-in. to the left and right of center of the target (identified as pinducers 2 and 4 in Figure 6). The radial pinducer locations were moved so that the gauge element was centered relative to the thickness of the PBX 9501 cylinder. The back of the target was also drilled and tapped with 1/8 in. NPT for Swagelok® fittings with Teflon ferrules for the pinducers and a compression fitting for the thermocouple. The thermocouple was evenly spaced between pinducers 1 and 3 on the back side of the target. The mild steel backing plate was drilled with three additional holes to accommodate the additional pinducers and the thermocouple on the back side of the target.

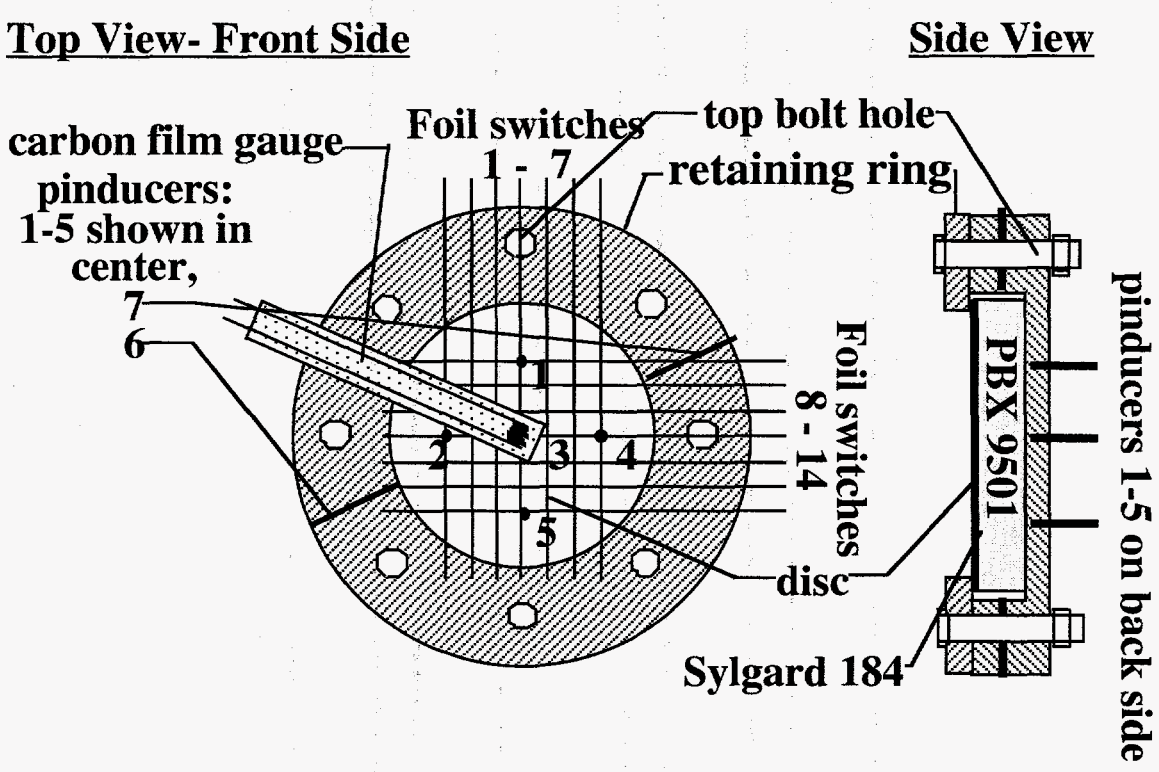

Figure 6: Live target design III, with 14 foil switches, one thermocouple, and 7 pinducers.

IV. DATA ANALYSIS AND RESULTS

A. Live Target Tests

Only the hit points were identified on unreacted target tests 1-4, while targets 5-10 contained a variety of diagnostics. For any target that did not react violently, front dent and rear surface deformation measurements were obtained by Don Murk and Roy Lucht using a scale and grid technique, and by George Harper using machine parallels and a depth gauge. These data are given in Table 4 for both the assembled and disassembled targets. The dent depth for the initial modeling analyses was arbitrarily defined to be the difference between the deepest point of the dent and the average of the measurements 40 mm to each side of that location. These data are given in Table 5. This information was used to calibrate and verify the materials models in the finite element DYNA2D calculations. Hit points, velocities, and reaction extent are also summarized in Table 5. Target test 3 did not result in a violent reaction. Afterwards, the target was disassembled, and a small hole was bored through the 0.125-in. ss cover plate at the center of the dent. After reassembly, the hole was packed with Detasheet, and a detonator was inserted. This allowed us to detonate all of the PBX 9501 in the target and compare the damage of the remains to that of an experiment where the target reacted violently. The remaining physical evidence from target 3 showed significantly more damage than any other target test that reacted violently, indicating that the low velocity spigot impacts only caused fast deflagrations or detonation of just part of the HE.

Table 4: Target dent data measured on assembled and disassembled targets.

Target #	Front (mm)[a]	Rear (mm)[a]	Front (mm)[b]	Front (mm)[c]	Front (mm)[d]	Front (mm)[e]	Rear (mm)[f]
3	13.0	1.0	(g)	(g)	(g)	(g)	(g)
4	15.5	2.9	16.2	15.9	15.0	15.6	2.9
6	17.3	4.1	17.7	17.4	17.0	17.2	3.6
8	17.0	4.3	18.6	18.3	17.4	18.0	4.7

[a] Measurement made on assembled target.
[b] Measurement made on disassembled target. Measurement was made on the front side of the 304 ss cover.
[c] Measurement made on disassembled target. Measurement was made on the back side of the 304 ss cover.
[d] Measurement made on disassembled target. Measurement made relative to the edges of the PBX 9501 surface.
[e] Measurement made on disassembled target. Measurement made relative to the front edges of the 304 ss holder. Thickness difference between the PBX 9501 and the holder was assumed to be 3.81 mm.
[f] Measurement made on disassembled target. Measurement made on back side of 304 ss holder.
[g] Target 3 was used in another test to identify the damage due to an intentional detonation of the PBX 9501.

B. Ferrite Scope Measurements

Measurements on the remaining 304 ss pieces of targets 3 and 5 were obtained by Mike Lopez using a Fisher Ferrite Scope instrument and probe. These are shown in Figure 7 and Figure 8. Measurements on the fragments from target 3 were obtained after the PBX 9501 was detonated. The measurements indicate that parts of the targets experienced high strain during the violent events produced by the reaction of the PBX 9501. The result of the shearing is believed to be the conversion of the austenitic phase of the 304 ss to the martensitic phase. Karl Staudhammer had previously made ferrite scope measurements on 304 ss samples that had undergone low strain rate deformation, and he evaluated each sample to determine the percentage of martensitic phase present after the deformation. He used this data to develop the calibration curve shown in Figure 9. Even though the target pieces experienced a high strain rate deformation, unlike his samples, the calibration curve still can be used to roughly approximate the extent of phase transition in the ss due to the violent event. One might have expected that the target pieces from the PBX 9501 detonation test (see Figure 7) would have experienced a higher degree of phase transition as compared to those of a violent reaction (see Figure 8) with little or no detonation. However, a comparison of the ferrite scope measurements shows that the target 5 data exhibits measurements indicative of higher shear induced more uniformly across the back cover plate than the target 3 data.

Table 5: Live target data summary.

#	Test Label	Target Geometry	Velocity (ft/s)	Velocity (mm/μs)	Results
1	DF15-803	I	–	–	•Impacted retaining ring.
2	DF15-2319	I	278.6	0.0849	•Violent reaction.
3	DF15-2325	I	185.6	0.0566	•No reaction. 12.6 mm dent[1], ~1 mm deformation of back plate. •Impact 1.0 in. high.
4	DF15-2330	I	214.9	0.0655	•No reaction. •14.2 mm dent[1], 2.9 mm deformation of back plate. •Impact 0.375 in. high, 0.375 in. left.
5	DF15-2347	II	264.9	0.0807	•Violent reaction. •Impact 0.6-in. low, 0.22 in. left (from active grid).
6	DF15-2368	II	232.6	0.0709	•No reaction. •15.2 mm dent[1], 4.1 mm deformation of back plate. •Impact 0.5 in. low.
7	K3-1235	III	250 ± 5	~0.0762 ±0.002	•Violent reaction. •Impact 0.25 in. low, 0.25 in. right (from active grid). •Velocity estimated based on previous tests; instrumentation failed.
8	K3-1278	III	237.0	0.0722	• No reaction. •17 mm dent[2],4.3 mm deformation of back plate. •No pinducer or thermocouple data; data acquisition failure. •No carbon foil gauge.
9	K3-1290	III	246.3	0.0751	•Semi-violent reaction.[3] • Impact on center (from active grid). • No carbon foil gauge. • Radial pinducers set in contact with PBX 9501.
10	K3-1304	III	325 ± 5	~0.0991 ±0.002	•Violent reaction. •Impact within 0.5-in. of center (from active grid). •Radial pinducers set in contact with PBX 9501. •Velocity estimated based on previous tests, instrumentation failed.

[1]The dent depth for the initial modeling analyses was arbitrarily defined to be the difference between the deepest point of the dent and the average of the measurements 40 mm to each side of that location.
[2] Defined as maximum dent depth relative to the entire front surface of the cover plate.
[3] "Semi-violent reaction" is in reference to a test result where part of the PBX 9501 energetic material was recovered from the test.

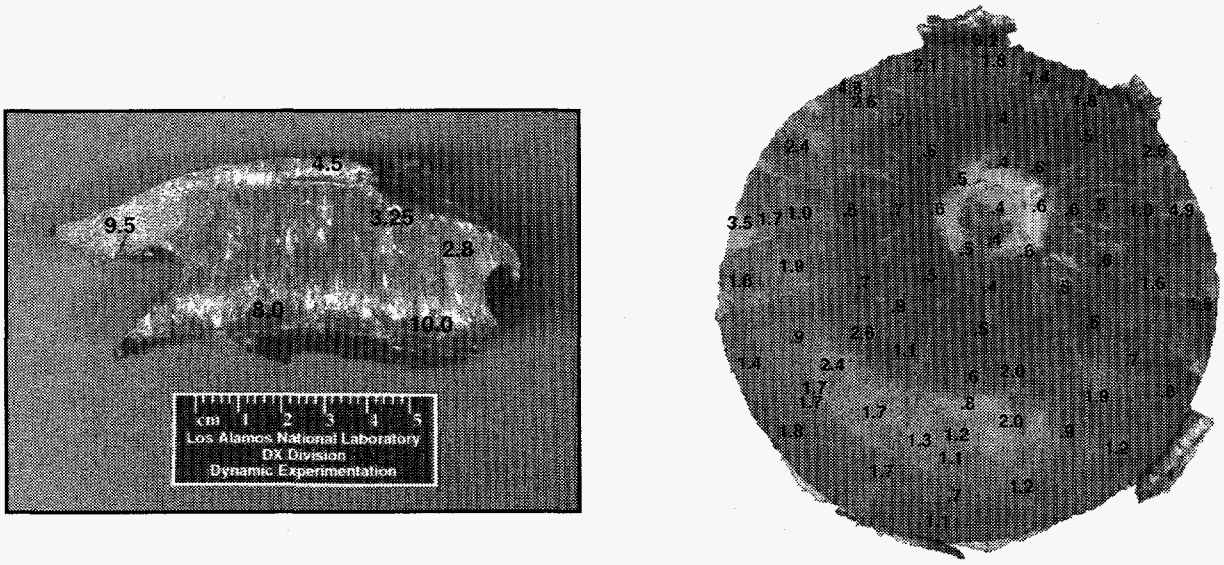

Figure 7: Ferrite scope measurements on target 3 (DF15-2325) fragments, post test, after intentional detonation of PBX 9501.

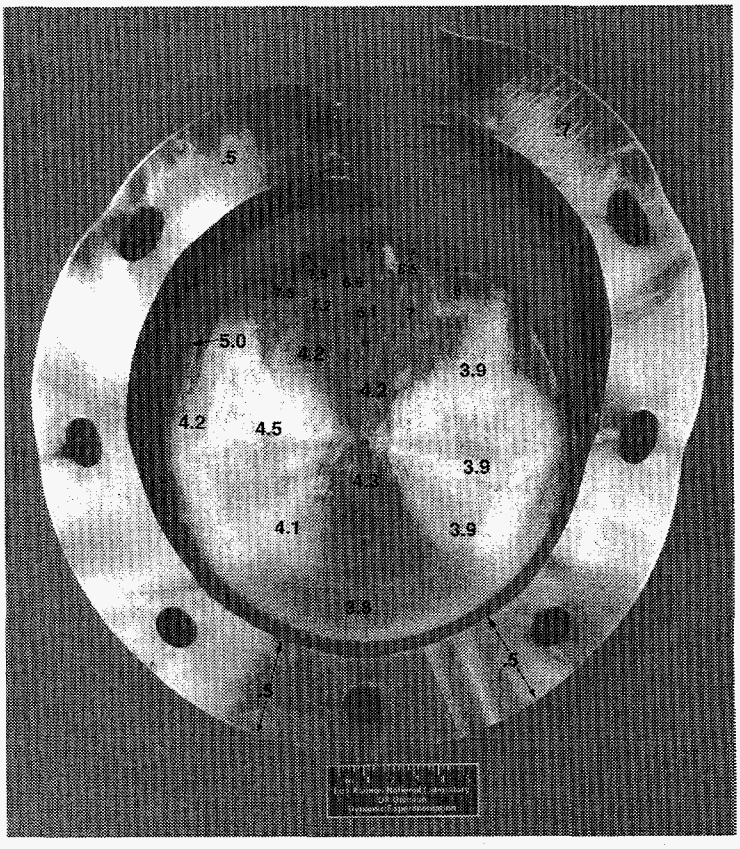

Figure 8: Ferrite scope measurements on target 5 hardware, post test.

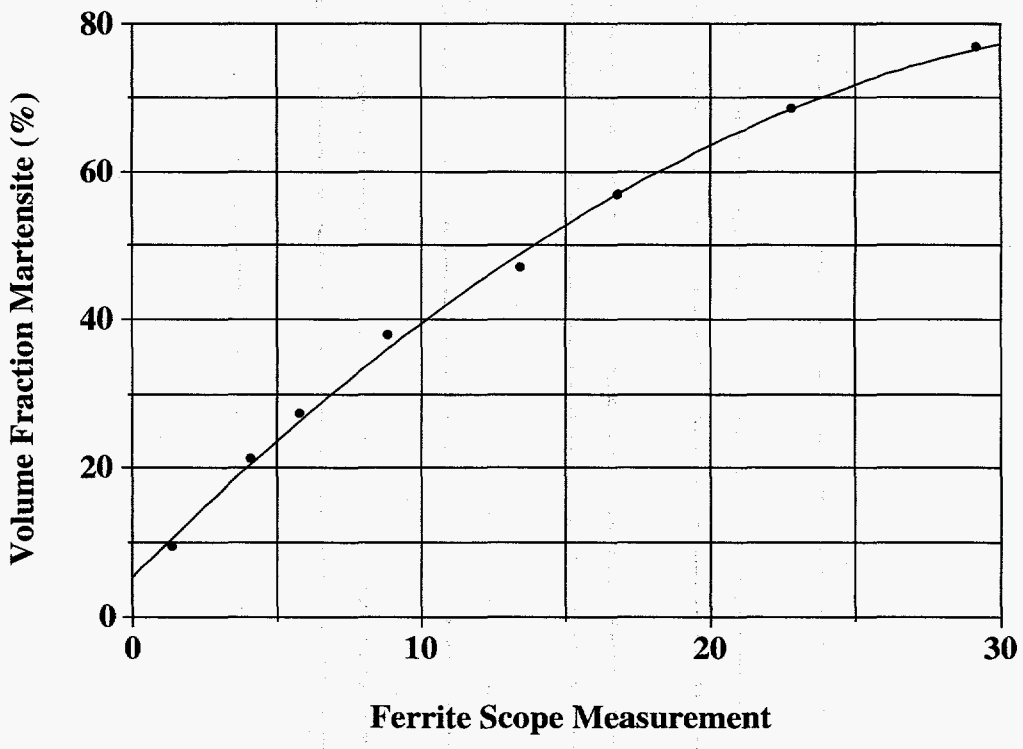

Figure 9: Karl Staudhammer's ferrite scope data on 304 ss.

C. Instrumented Target Results

The light/photodiode velocity boxes described earlier worked quite well and yielded velocities estimated to be accurate to better than one percent. However, on two experiments the digital oscilloscopes apparently were triggered by CDU noise, and we did not record the velocity data. Nonetheless, we have an excellent data base of tests completed with the same and/or similar powder loads on the same barrels as the tests in question. Therefore, we can estimate the velocities with reasonable confidence. The velocity was estimated at 250 ±5 ft/s and 325 ±5 ft/s for target tests 7, and 10, respectively.

Data from target tests 5, 6, 7, 9 and 10 are shown in Figures 10 to 14; unfortunately, instrumentation data from target test 8 were lost. In the first two target tests, 5 and 6, the side radial pinducers, 4 and 5, were too short to extend beyond the outside of the ss side wall, thus, making a good ground connection between the cable and pinducer was difficult. Also, for all of the instrumented tests, it was difficult to make a solid connection of the cable to the pinducer because of the connector design. After impact, the shock wave and reflections ran through the target and were followed by the buildup of reactive waves in some cases. These mechanical vibrations produced intermittent connections of the cables to the pinducers. The noise was artificially removed for the presentation in the figures by smoothing the data over 20 points making the effective time resolution 800 ns/point. To try to avoid this problem, we soldered the connections onto the pinducers for the last two tests and achieved some degree of success (although not complete). Because the soldering could not be done safely with the pinducers in contact with the HE, all of the pinducers had to be removed, soldered, and reinstalled. Reinstallation of the side radial pinducers on the last two targets placed them in direct contact with the PBX 9501, in contrast to the positioning of the radial pinducers for the first four instrumented tests.

Figure 10: **Target 5, experimental data, DF15-2347**
20-April-1995 264.9 ft/s - Violent Reaction

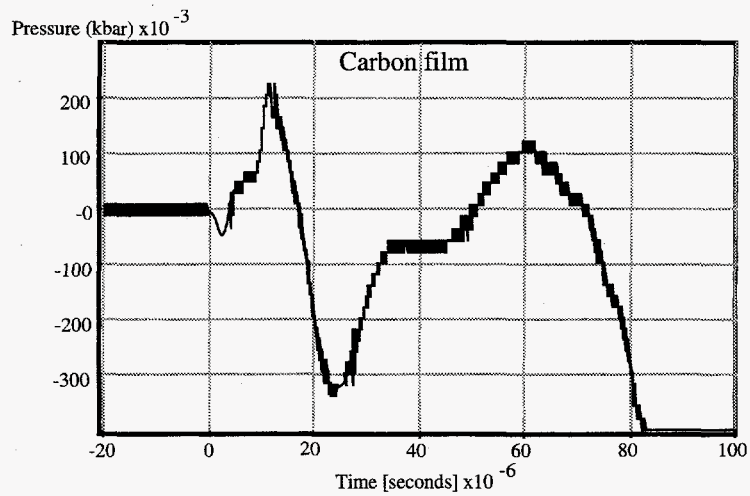

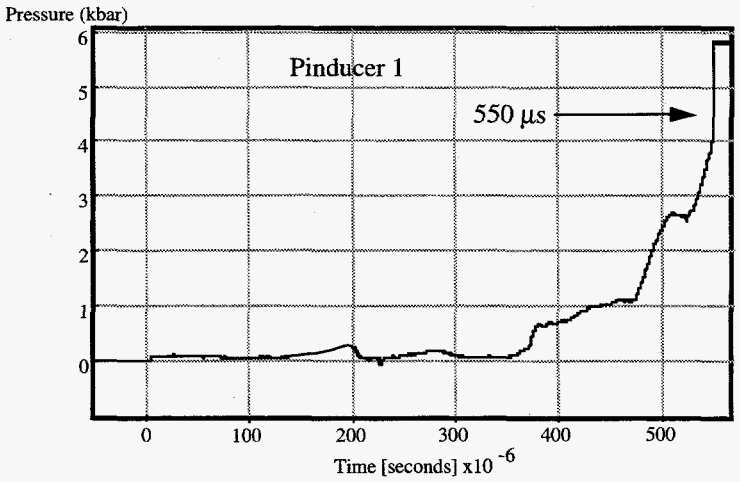

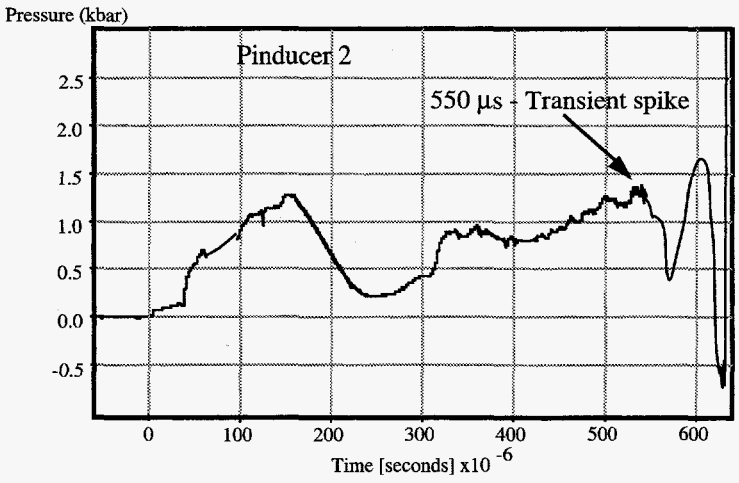

Figure 10: **Target 5, experimental data, DF15-2347 (continued)**

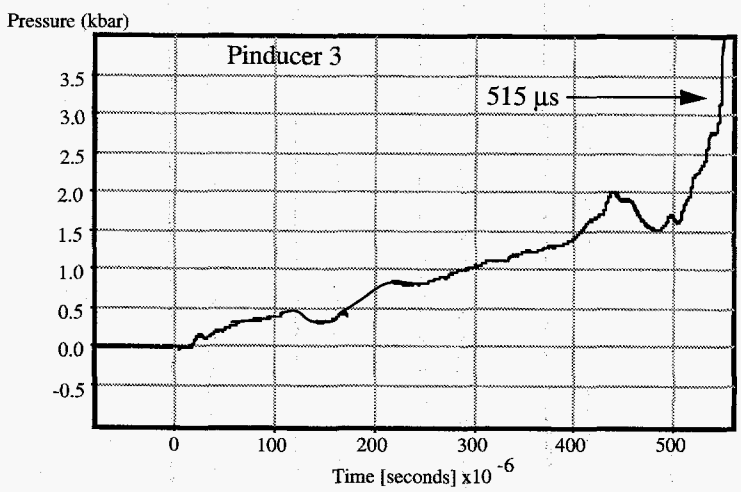

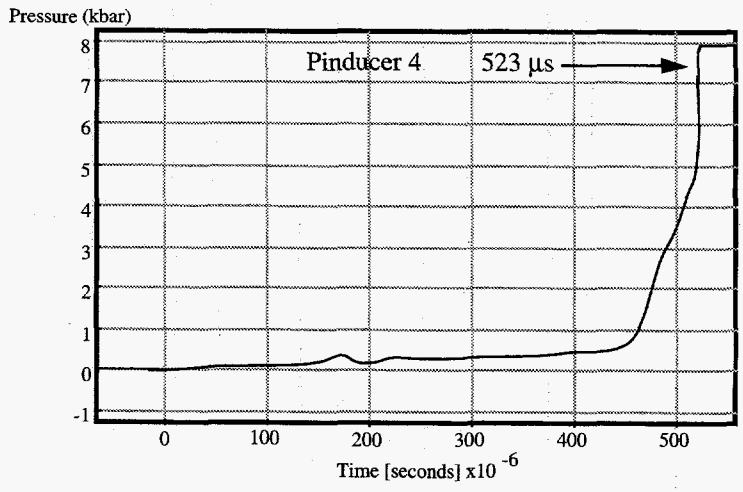

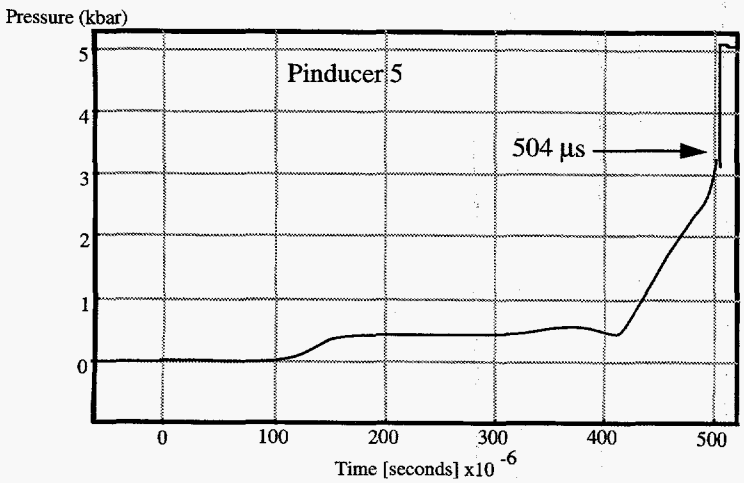

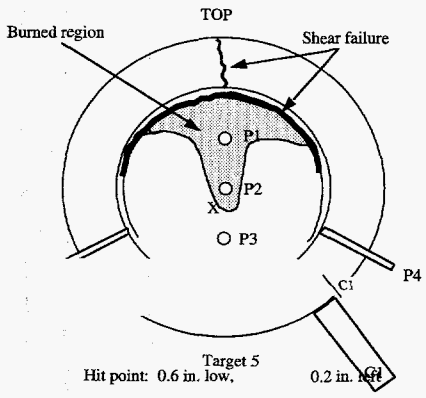

Target 5
Impact point: 0.6 in. low, 0.2 in. left

Figure 11: **Target 6, experimental data, DF15-2368**
232.6 ft/s - No Reaction

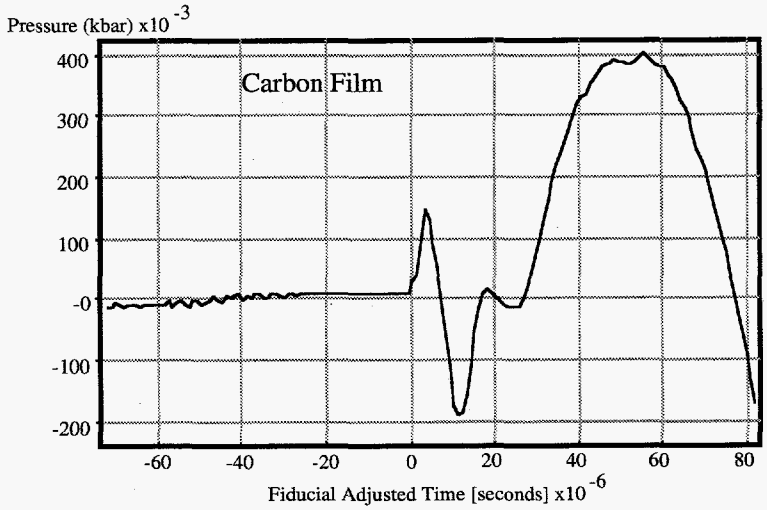

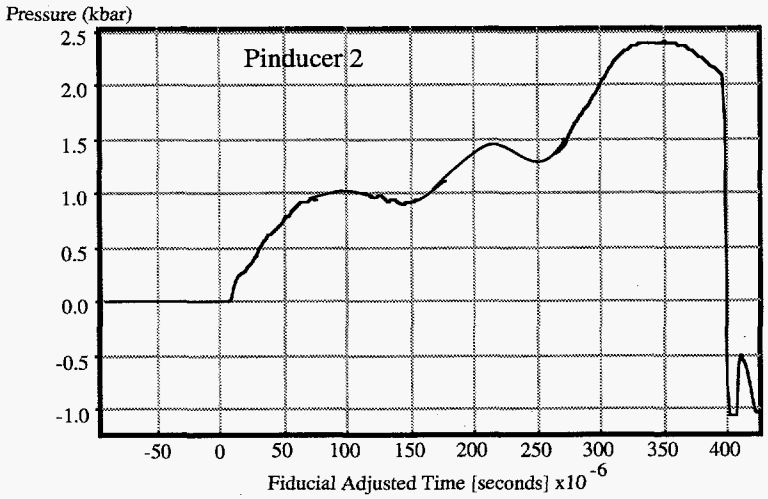

Figure 11: **Target 6, experimental data, DF15-2368 (continued)**

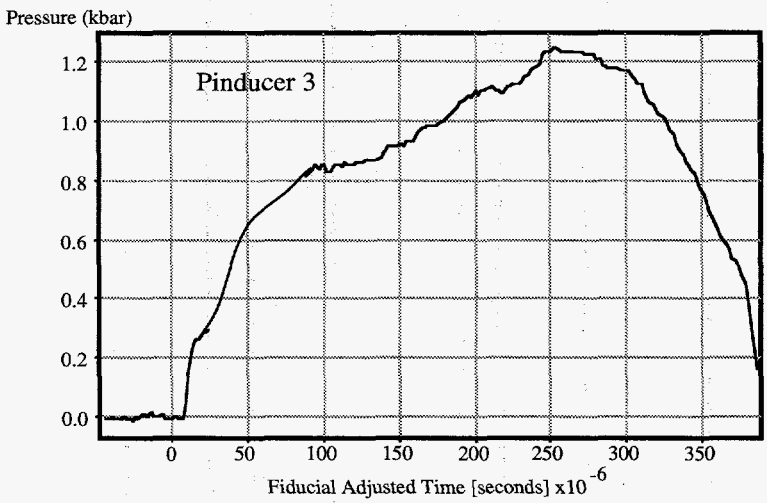

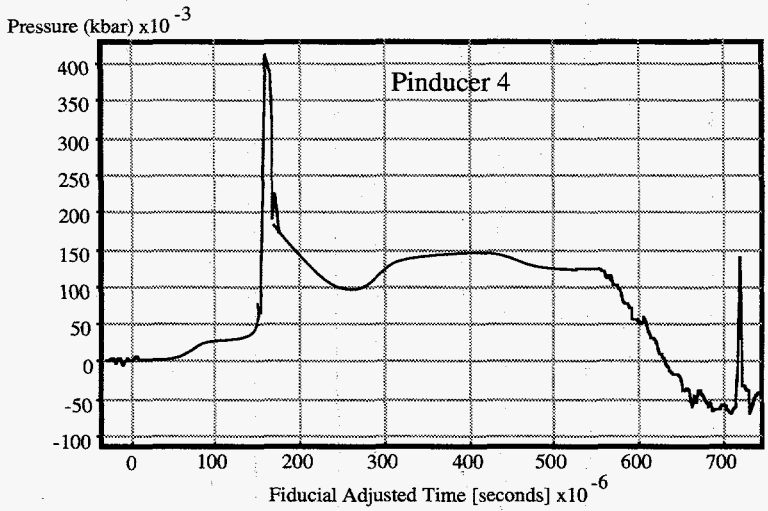

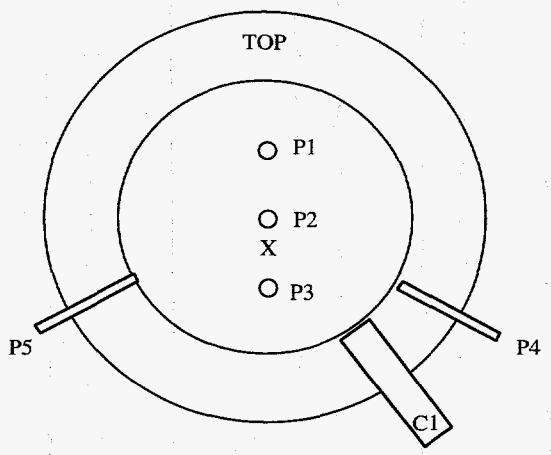

Target 6 Impact point: 0.5 in. low

Figure 12: **Target 7, experimental data, K3-1235**
27-November-1995
250±5 ft/s - Violent Reaction

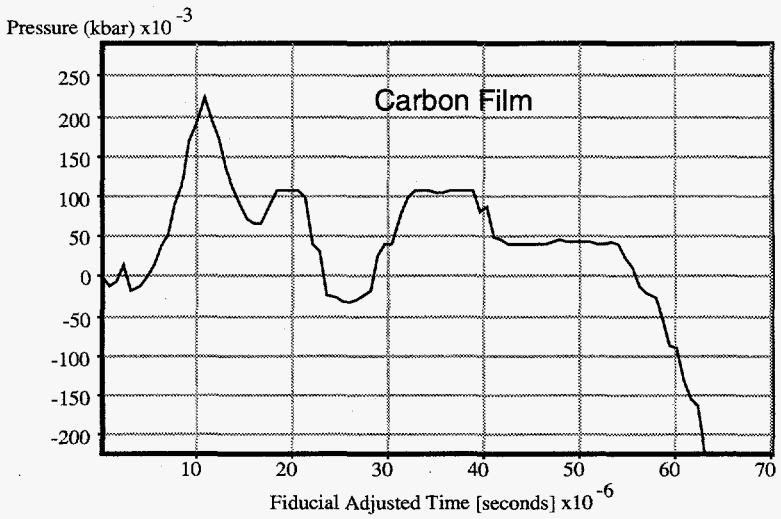

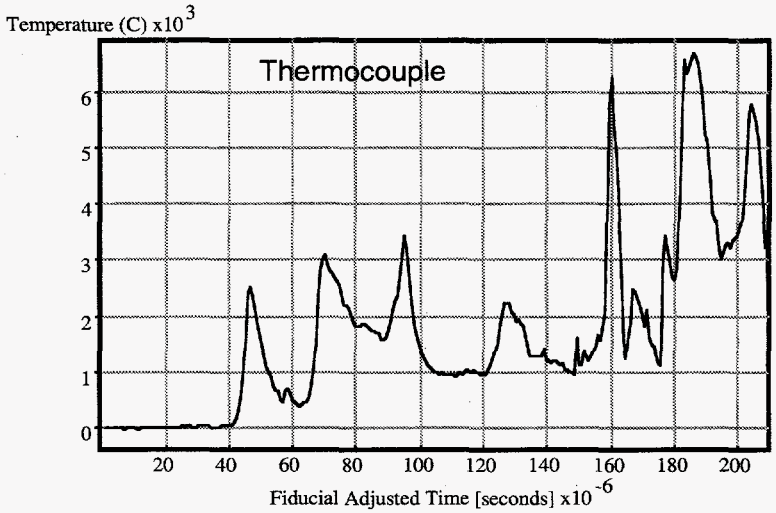

Figure 12: **Target 7, experimental data, K3-1235 (continued)**

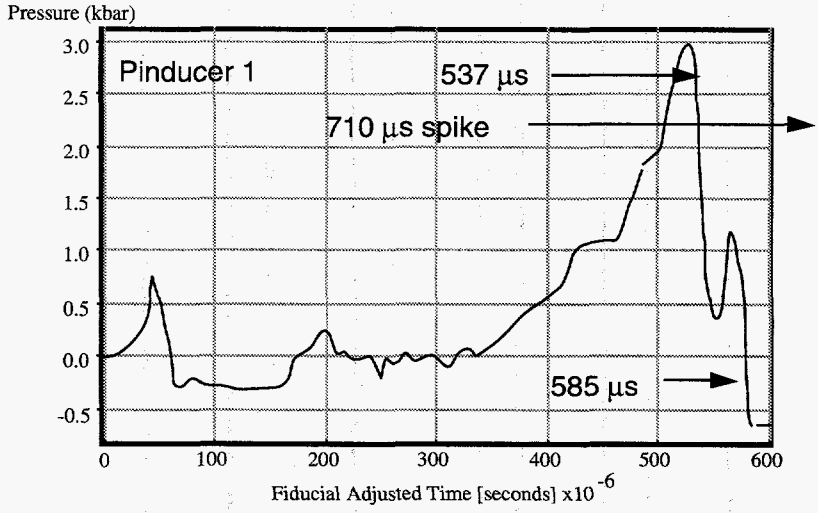

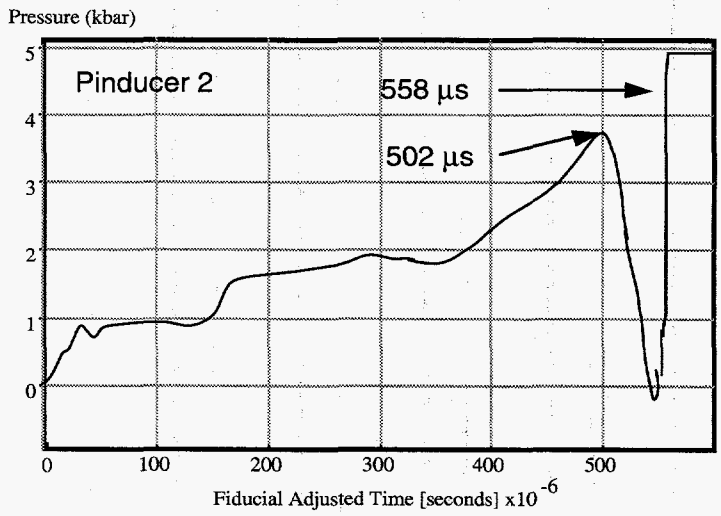

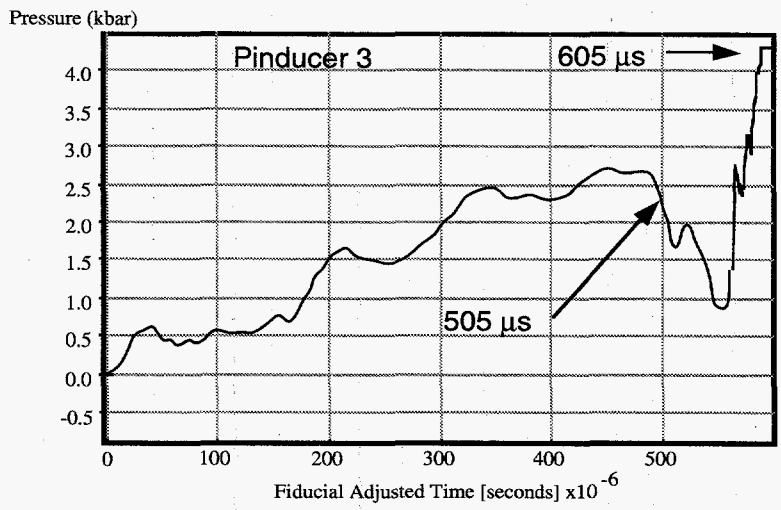

Figure 12: **Target 7, experimental data, K3-1235 (continued)**

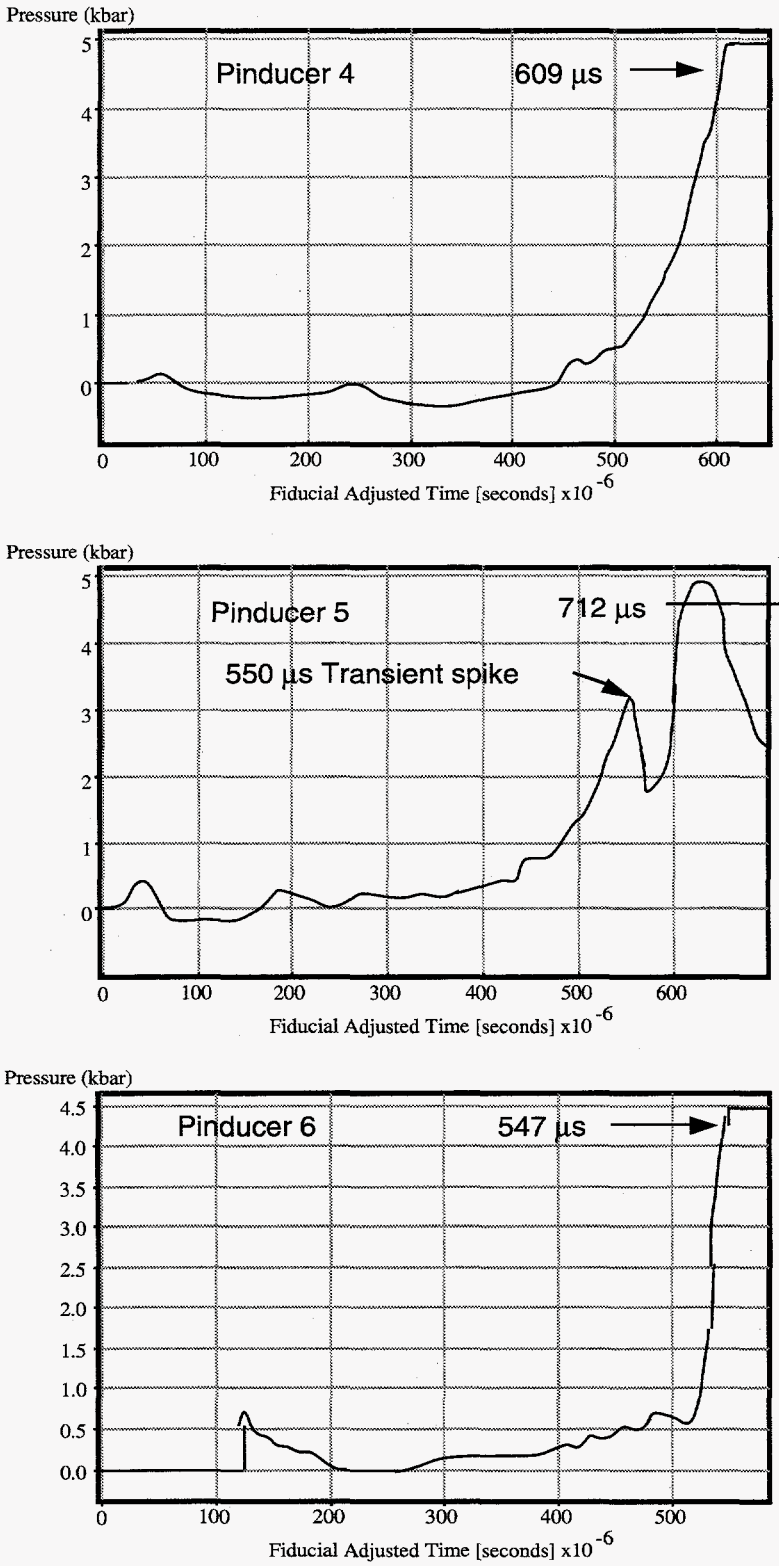

Figure 12: **Target 7, experimental data, K3-1235 (continued)**

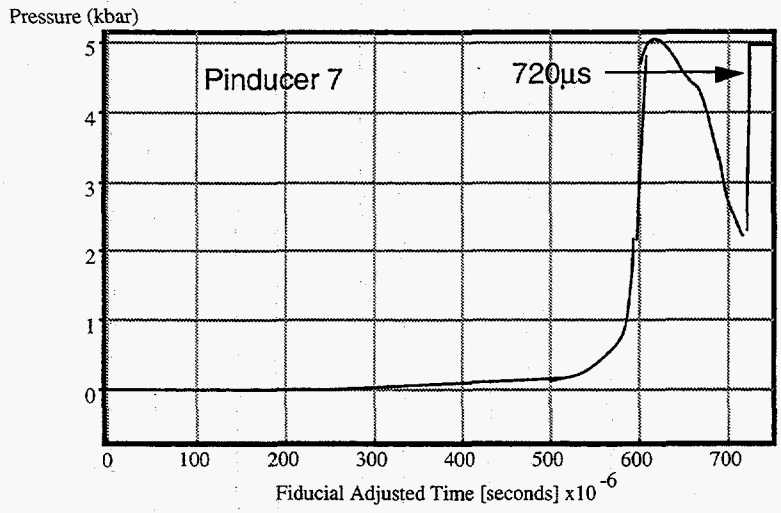

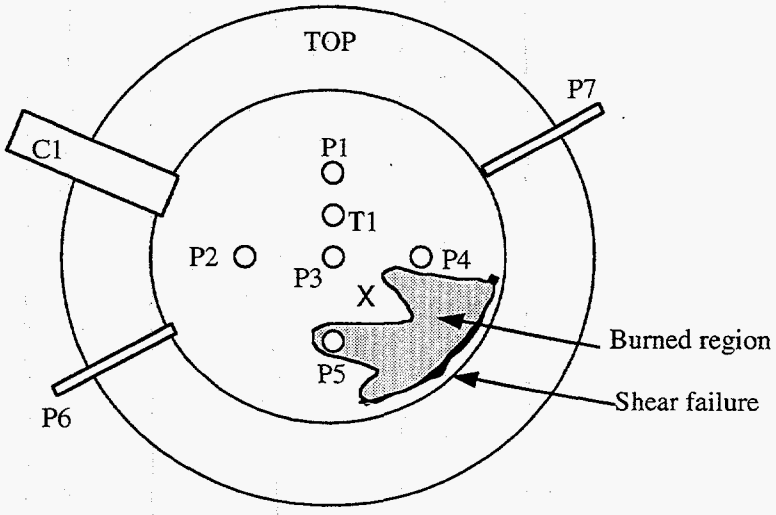

Target 7
Impact point: 0.25 in. low, 0.25 in. right

Figure 13: **Target 9, experimental data, K3-1290**
27-November-1995
246.3 ft/s - Semi Violent Reaction

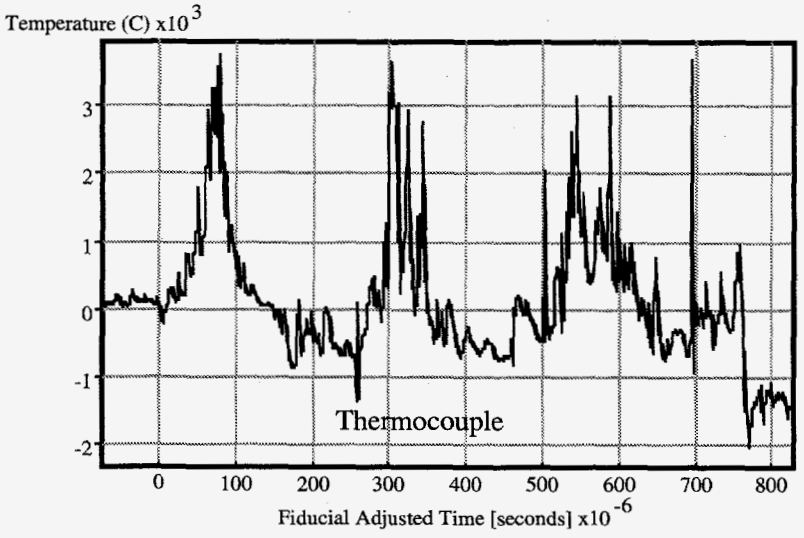

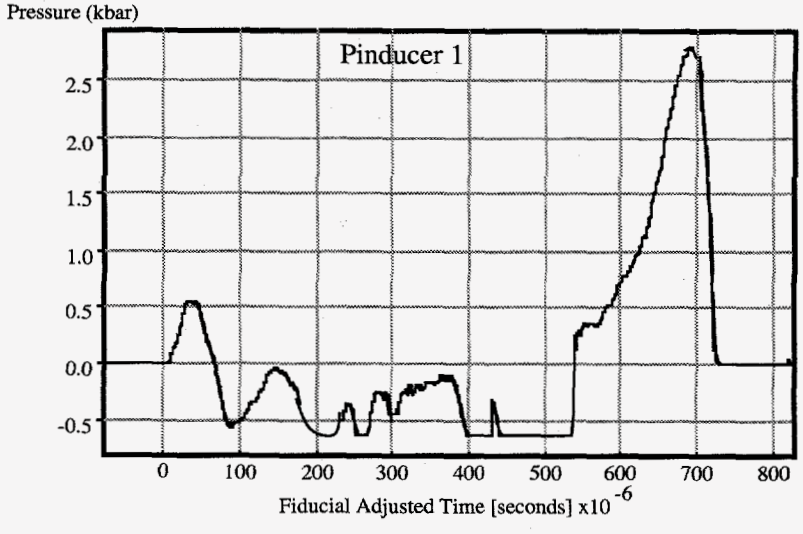

Figure 13: **Target 9, experimental data, K3-1290 (continued)**

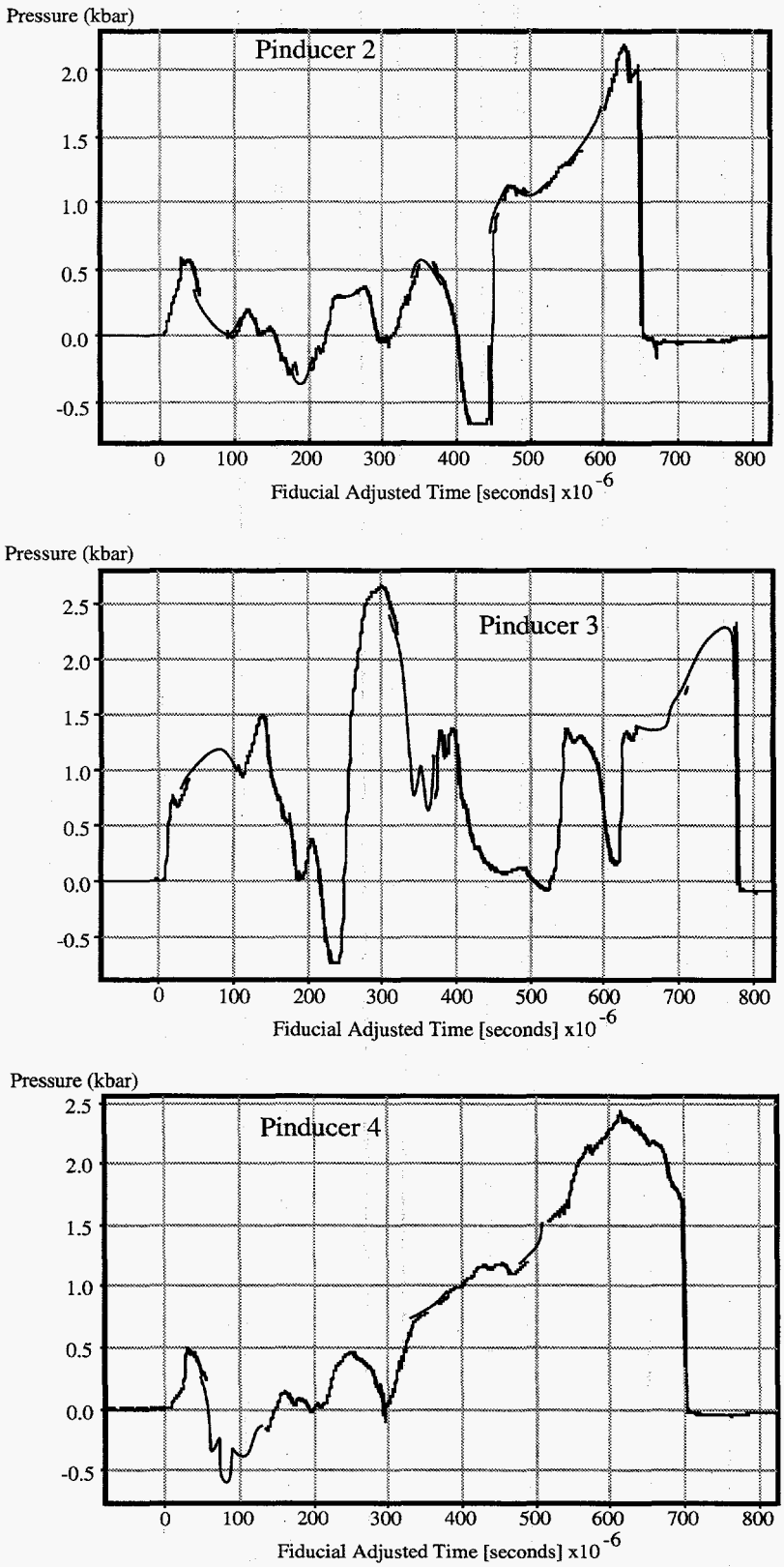

Figure 13: **Target 9, experimental data, K3-1290 (continued)**

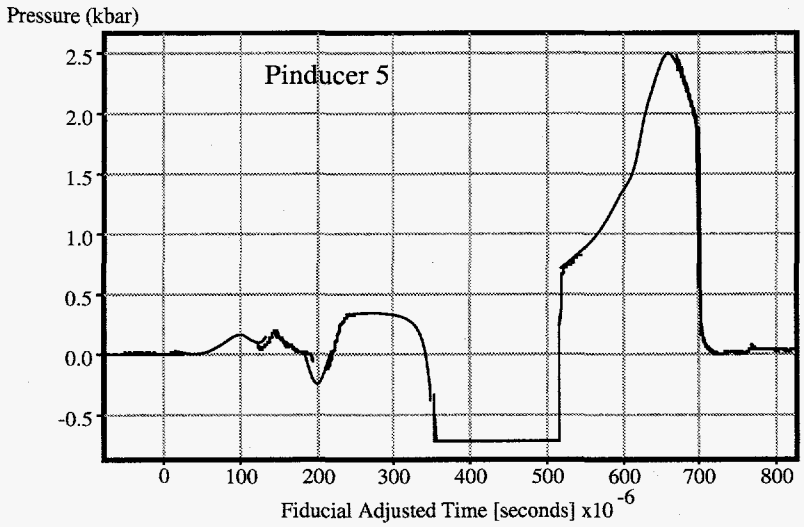

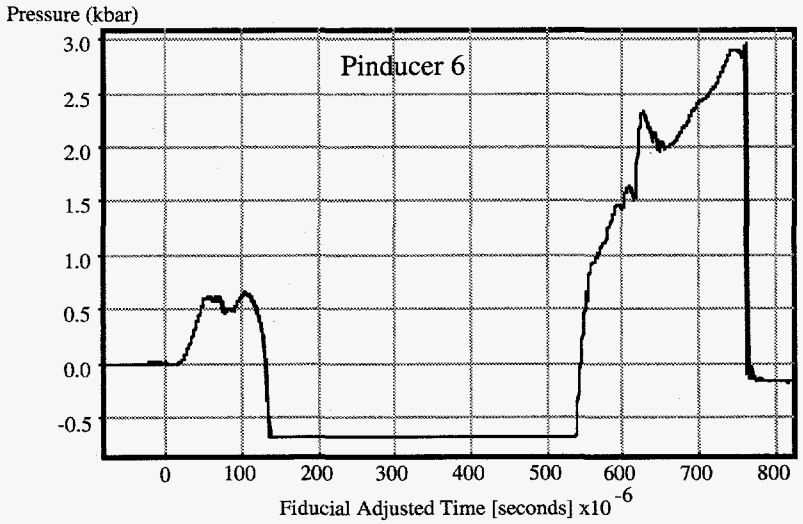

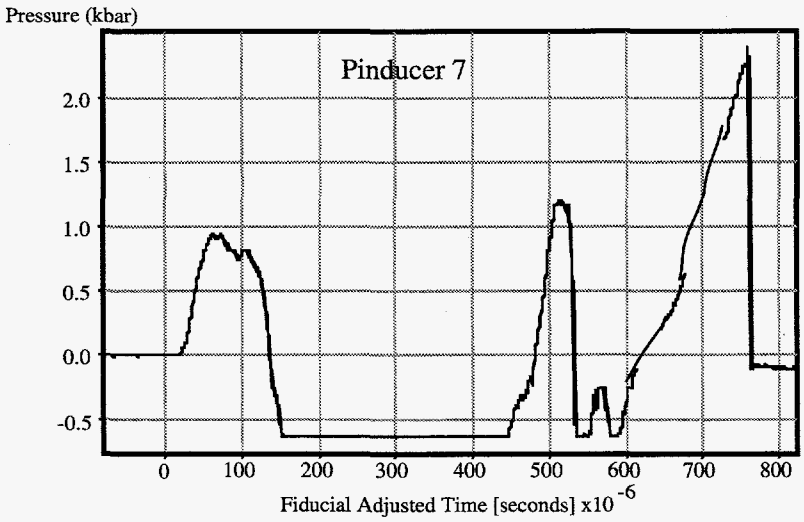

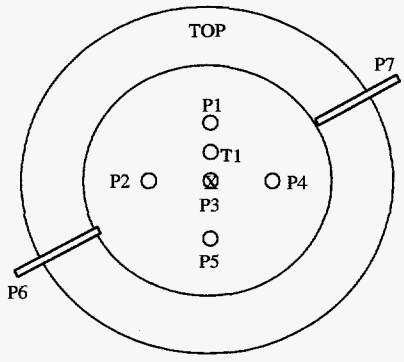

Target 9
Impact point: center

Figure 14: **Target 10, experimental data, K3-1304**

15-December-1995

325±5 ft/s - Violent Reaction

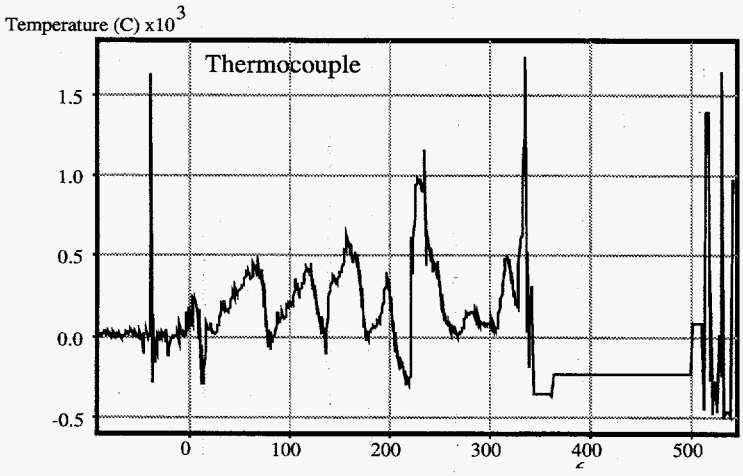

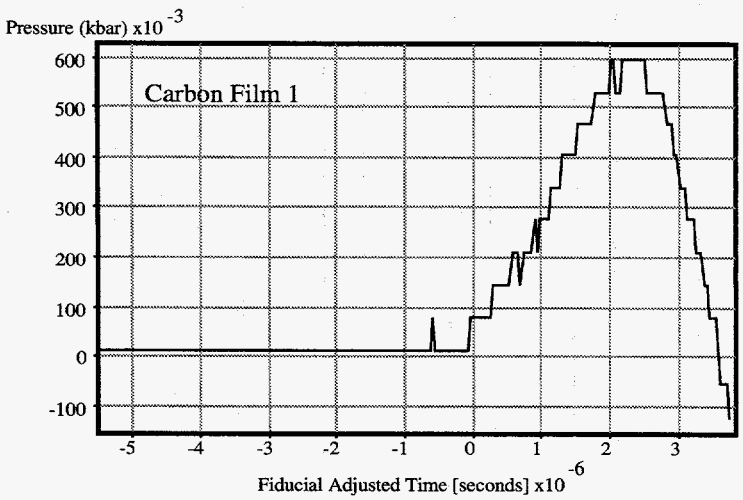

Figure 14: **Target 10, experimental data, K3-1304 (continued)**

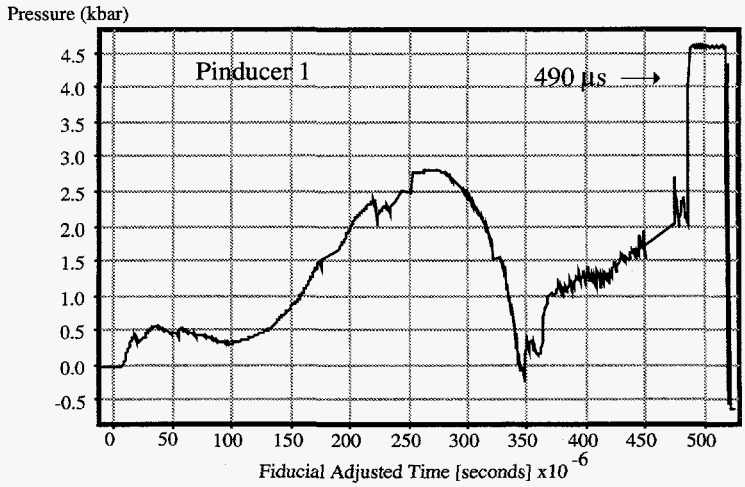

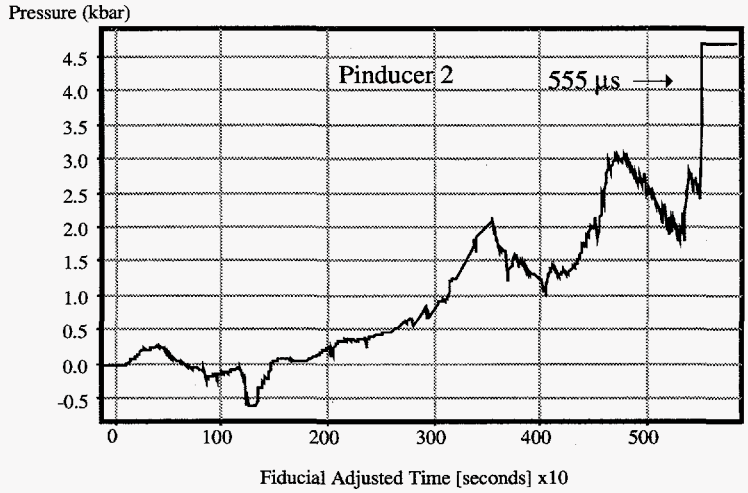

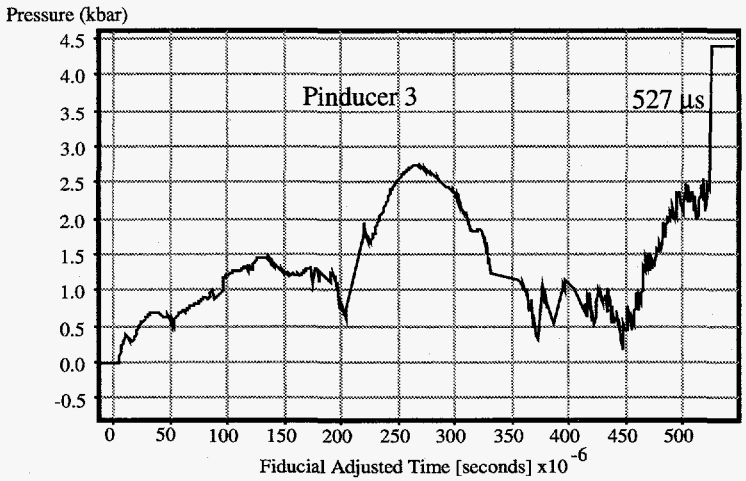

Figure 14: **Target 10, experimental data, K3-1304 (continued)**

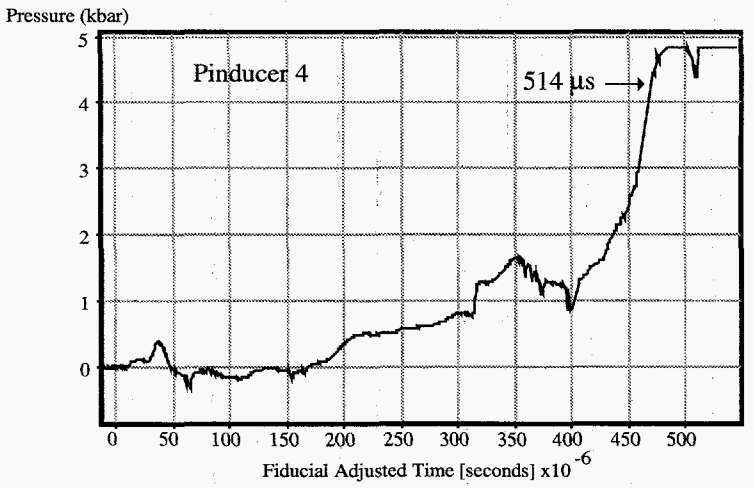

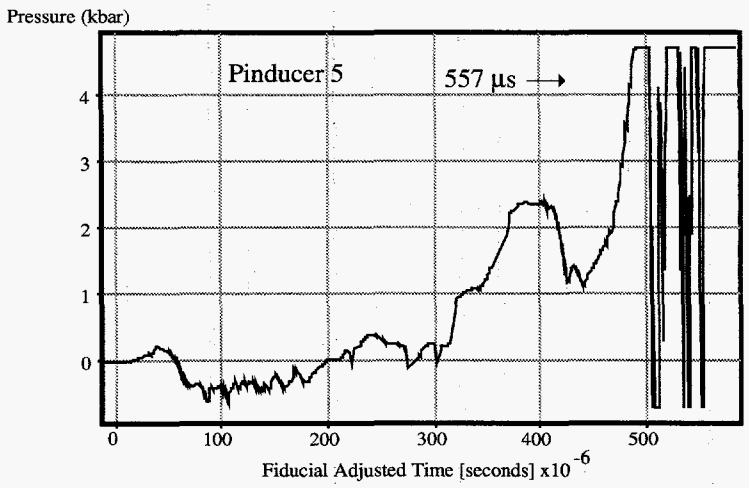

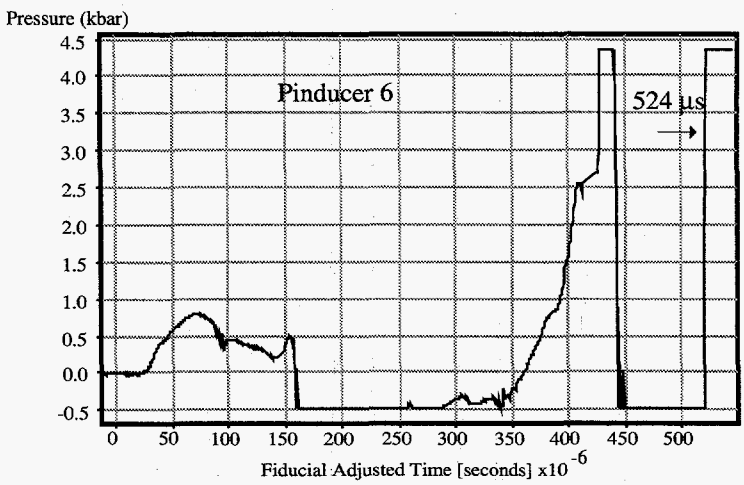

Figure 14: **Target 10, experimental data, K3-1304 (continued)**

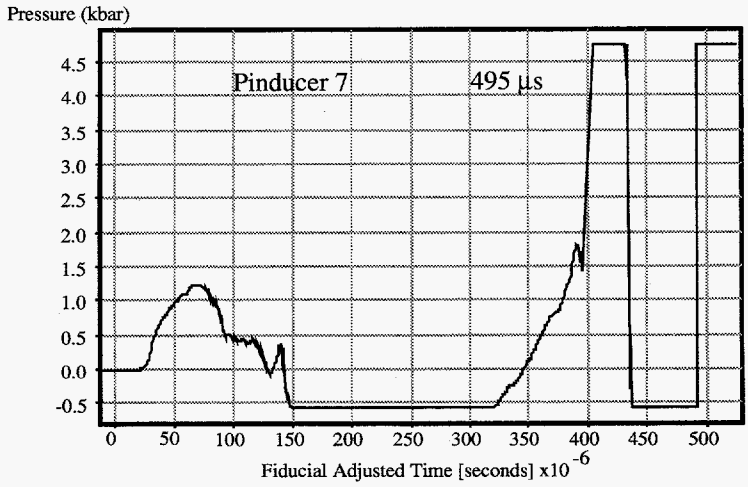

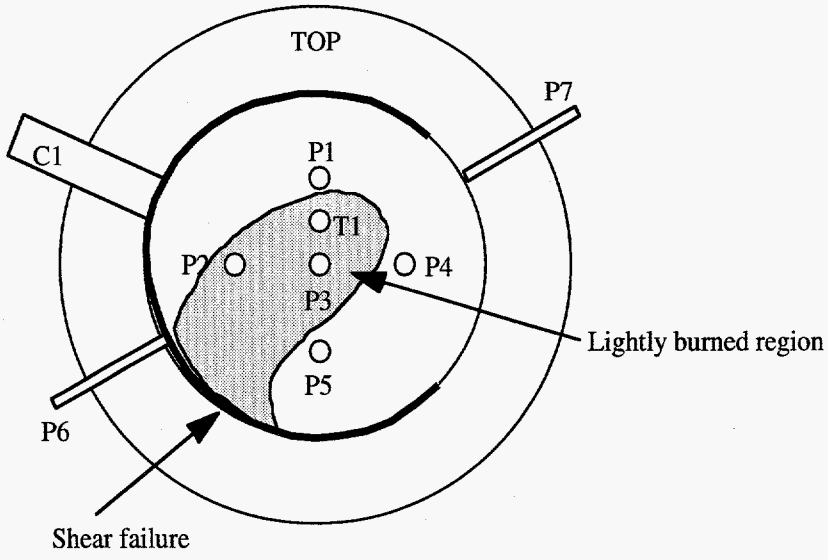

Target 10
Impact point: Within 0.5 in. of center

As stated previously the three rear surface pinducers in targets 5 and 6 were glued into tight fitting holes with their active element surfaces flush with the back inner ss surface prior to complete target assembly. In the last four tests, the back of the target was drilled and tapped with 1/8 in. NPT for Swagelok® fittings for the pinducers and a compression fitting for the thermocouple. The gauges were then installed after the rest of the target was assembled with the PBX 9501. The position of the front surface of the gauges may have varied a few ten thousandths of an inch from test to test in these cases; however, we do not believe that this significantly affected the data because the total available area for heat transfer and stress wave propagation could not have changed appreciably.

The pinducers and carbon film gauges were all nominally 50Ω gauges and decreased in resistance with increasing pressure, but they also increased in resistance with increasing temperature. The gauges were used with a bridge circuit (Dynasen pulsed power supply) to measure resistance changes as a function of time. The applied voltage was ~70 V and the signal-to-noise ratio decreased with decreasing voltage. The power dissipation in these gauges is V^2/R so either a pulsed power supply or very low applied DC voltage is required to avoid ohmic heating and destruction of the gauges. For example the 1/4 watt pinducer could only withstand about 3 VDC, and the thin carbon film gauge only a small fraction of a volt. We chose to keep the high signal-to-noise ratio and use the pulsed power supply; however this caused significant timing problems.

Our standard triggering techniques of foil switches, break wires, etc. were not effective because of the slow velocity of the projectile and stretching of the switch material. The pulsed power supply channels have pulse widths of 800 to 1100 μs. Impact time to XDT time was found to be in the 500 to 1000 μs range, requiring triggering to be within better than ±100 μs. On the first two instrumented tests we used a double wire grid. The two grids were separated by 0.5 in. and were perpendicular to each other. The first grid was expected to stretch and contact the second grid with the resulting short providing a trigger. This system seemed to work well on the first test but less satisfactorily on the second.

Next, we constructed a three-path grid using the light sources and photodiodes used in the velocity box. However, the supporting electronics were not adequate to provide reliable triggering. Triggering of all these systems was typically tested by dropping the spigot through the trigger ring to get the supporting electronics optimized, and then by firing the gun at an inert (plywood) target. The next system we tested used light emitting diodes and photodetectors with built-in amplifiers mounted in a three-path configuration. This system produced large sharp trigger signals; however, it occasionally produced triggers significantly before the projectile could block the light paths. We believe the slight permanent magnetism of some of the spigot projectiles may have caused this apparent clairvoyant capability.

The final solution was a ring with three graphite rods. Each rod was connected in series with enough resistance to make a total of ~50Ω. Each was connected to a velocity screen monitor (VSM), which produced a sharp pulse every time the projectile broke one of the graphite rods. The three VSM outputs were passed through a diode bridge to pick off the first one to provide a trigger for the diagnostics. This low technology solution has worked well and provided good reproducibility and reliability.

Because there was still about ±95 μs jitter in the trigger for the last experiments and more in the first two instrumented tests, we needed to establish a common time base for all of the data. All records had a fiducial marker that we set initially to a common time for each data set. If a data set had a reasonable carbon film gauge record, then the first response of the carbon film profile was set to $t = 0$, and all other records in that data set were shifted to the same time profile. Some experiments did not have carbon film gauges, and some did not give a reasonable response. In these cases, the time of the first response of the

pinducer centered in the back of the target was set to 9 μs, and all other records in that set were adjusted by the same amount. Nine μs is the approximate time required to traverse the 1-in. thickness of the PBX 9501 at sonic speed. Target tests 6 and 10 are referenced to the carbon film record. Target tests 7 and 9 used pinducer 3 as the reference. For target test 5, the fiducial was pulsed at zero time, which appeared to be coincident with the time of impact, so the time base shift was not required.

The data in Table 5 for the nonreactive experiments show monotonically increasing damage of the target with increasing impact velocity. It is also interesting to note that the velocity threshold for reaction is very sharp, and no crossovers have been observed. For many experiments involving XDT or other non-shock initiation processes (such as shotgun or Taylor series), there are often tests with velocities above the average threshold that do not react and ones below the threshold that do react. This is not the case here. In fact, the test near threshold velocity, target test 9, was only semi-violent. The estimated extent of PBX 9501 of reation for all 10 tests is shown schematically in Figure 15.

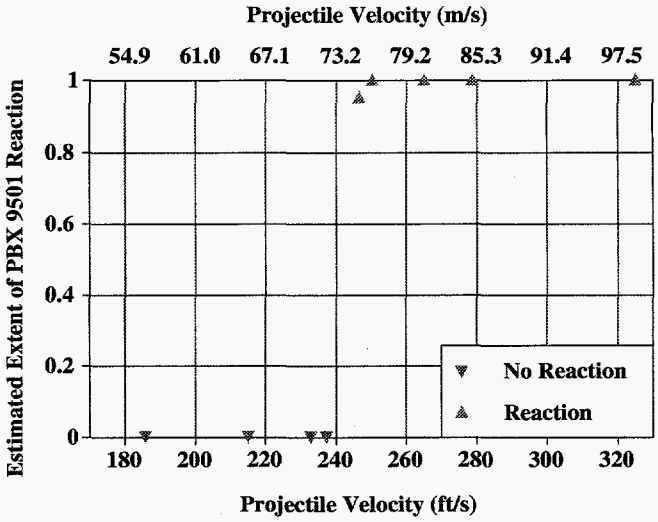

Figure 15: Estimated of extent of PBX 9501 reaction as a function of projectile velocity. A value of one is defined to mean that all of the PBX 9501 reacted in the test before going negative.

Studying Figures 10–14, some trends in the data can be observed:

1. The carbon film records show a rise from 0.1 to 0.5 kbar over 5 to 10 μs and then negative. In some cases, a later positive excursion in pressure is observed before the record goes negative again, clearly indicating the gauge is broken. The first negative excursion is usually less than -0.5 kbar and is probably due to a temperature increase in the gauge from compression heating, fracturing, and/or shear flow heating of the HE. The temperature effect can overwhelm the pressure effect for a while. As the pressure rises still further, it overcomes the heating, but the gauge breaks shortly thereafter, usually before 100 μs after impact. This explanation is consistent with increasing reactivity at increasing velocity. Target test 6, Figure 11, was at 232.6 ft/s and did not react violently. It shows only a small negative region, and the second positive region is quite large, indicating that the pressure effect has dominated over the temperature effect. The system did not react, so a large temperature effect should not be observed. Target tests 7 and 5 at 250 and 264.9 ft/s show a increasing temperature effect. Target test 10 at 325 ft/s showed the sharpest and highest rise in initial pressure, which is consistent with the highest impact velocity. It then quickly went negative and stayed off scale, which indicates a very strong temperature response, consistent with the highest velocity.

2. Next consider the damage to the targets shown schematically at the end of each figure where the instrumentation configuration is also shown. The extent of damage increases from almost nothing at low velocities to quite extensive at high velocities. However, as discussed earlier, even the highest velocity impact did not produce the level of damage and fragmentation to the target that prompt detonation did. Target test 9 near the velocity threshold showed no shear failure. The next highest velocity at 250 ft/s, target test 7, produced a small amount of shear failure and a small burned region on the inside of the back of the target. The next two velocities of 264.9 and 325 ft/s, target tests 5 and 10 respectively, produced about the same amount of shear damage and burning. At first this may seem inconsistent because 325 ft/s is significantly larger than 264.9 ft/s; however, it may be that the level of damage is limited once the target confinement material fails, releasing the pressure and quenching the reaction.
3. The fast thermocouples did not yield much useful information. These chromel-alumel thermocouples are only calibrated up to about 1400°C, but the voltages measured correlate to temperatures much higher than that if the calibration is extrapolated. The thermocouple is made to respond fast by vapor-coating the junction of the two materials on the end of a thin coaxial arrangement of the chromel and alumel. It is likely that the flow of HE along the back plate of the target quickly removed this junction and basically left an ionization pin in its place. If this explanation is correct, then the initial fast rise of the temperature may be correct. However, beyond 1400°C we are probably observing regions of hot, ionized, reacting material flow over the remaining ionization pin. This would account for the higher than expected voltages and the rapid slope changes.
4. The time to violent reaction can be roughly deduced from the pressure profiles. A positive spike near the end of the trace indicates near zero resistance that could be caused by a strong shock or the gauge starting to move and the leads shorting out. A negative spike (in pressure) can only be caused by the gauge or leads breaking, causing an open circuit. This was not observed frequently on the pinducers in these experiments, although it is a common occurrence when thin foil gauges are used in shock experiments. Thus, it appears that the gauges remained active for most of the time of interest, although we did have the intermittent connection problem described earlier. Looking at the remaining target evidence, it is clear that at some point, the pressure was sufficient to push the pinducers out of the target. Because we often see reasonable signals for 500 μs to 1 ms in these tests, we postulate that the pinducers do not release until the fast deflagration or partial detonation starts.
5. The negative pressure regions of the profiles can be caused by high temperature or by an intermittent connection. If the gauge is momentarily disconnected, the negative region goes off scale even on the low amplification digitization record. However, if temperature is causing the negative region, the excursion is usually limited and can be seen on the low amplification record. It should be noted that Figures 10 to 14 show only the high amplification records because the signal-to-noise ratio is generally better. Radial pinducers 6 and 7 on target tests 9 and 10, for example, show a fairly broad negative region in the middle of their records. These were the radial pinducers that were positioned in direct contact with the outer circumference of the HE cylinder. The HE had to flow around the pinducers and basically encased the entire sensitive regions, potentially subjecting them to a significant thermal bath. Eventually the pressure rose sufficiently to overcome the temperature effect, and a rapid rise was observed before the system transited to violent reaction or detonation. Other gauges show the same effect to a lesser extent because most of the gauge was embedded in the ss back plate of the target, and only the front surface was subjected to the high temperatures. Examples of this include most of the gauges on target test 9, where the HE reacted semi-violently after a delay, gauges 1 and 5 on target test 7, and gauge 5 on target test 10. In general, the pinducer directly below the impact point never went negative, presumably because this region supported a continuing high pressure that always overcompensated for the temperature rise.

6. As the impact velocity increases, the pressure profiles show more clearly and consistently the transition to violent reaction or detonation. We know that at lower velocities the damage to the target is not extensive or uniform; thus it is reasonable that not all the pressure gauges show a clear transition. It is also reasonable that the times of transition (or gauge destruction) occur over more than 100 μs for velocities near threshold as in target test 7. This test at 250 ft/s was very near the velocity threshold and showed very little target damage. In comparison, target tests 5 and 10 were well above the threshold and showed substantial target damage. Almost all gauges for either test show transition within 50 μs or less. The wave velocities in these cases are of the order of 1 to 2 mm/μs, which would indicate a very fast deflagration, but not a high order detonation. It is also interesting to note that for these two experiments and perhaps also target test 7, the wave appears to start near the region of minimal target damage and propagate toward the region of maximum damage and burn. This indicates that the reaction needed to run for a while before it could develop sufficient pressures to cause the observed shear failure and develop sufficient temperatures to scorch the metal. For comparison, consider target test 9. Unfortunately, we ran out of recording time because the pulsed power supply turned off before the end of the experiment. However, pinducers 4 and 5 and perhaps 2 show the pressure turning over just before the record ended. It is possible at this velocity, which is so close to the threshold, that the burning caused sufficient pressure for the target to disassemble without producing a reactive wave. A volumetric burst without a strong propagating wave would explain the lack of shear damage to this target.
7. The pressure profiles from target test 6, which did not react, show a rise and fall of pressure (pinducer 2 was clipped by the power supply, but it had also turned over) with no negative regions on the pinducer records. This is just what is expected of an impact that is not strong enough to produce a self-sustaining reaction. The other experiments at least partially reacted, and generally showed significant rises in pressure near the end of the experiments. The time to violent reaction or target rupture decreases roughly from >750 μs to 600 to 550 to 525 μs as the velocity increases from 246.3 ft/s to 250 to 264.9 to 325 ft/s, respectively. A shock-to-detonation transition (SDT) that ran for 1 in. would take ~3 μs, so the processes involved are clearly very different.

D. Preliminary Analysis of Damaged PBX 9501

Photographs of the damaged HE from the tests that did not react are shown in Figures 16 and 17. Distinct crack patterns are observable in four regions. First, there is a clear region of compressed HE under the impact point of the projectile nose. The closed, circular cracks in this region, Region C, are difficult to see in the picture. Moving out radially, the next region, Region M, is composed of a fairly even mix of circular and radial cracks that coincide with the shoulder of the projectile. From this region, progressing to within a few millimeters of the holder wall, radial cracks dominate in Region R. The final region, Region D, is a single circumferential crack that runs a fairly constant distance from the holder wall of approximately 3 mm. The HE appears to be pushed radially from the impact region to expand into the annular void region, which increases the effective circumference at any given radial distance. Apparently, this stretching exceeds the tensile strength of the PBX 9501 and produces the radial cracks.

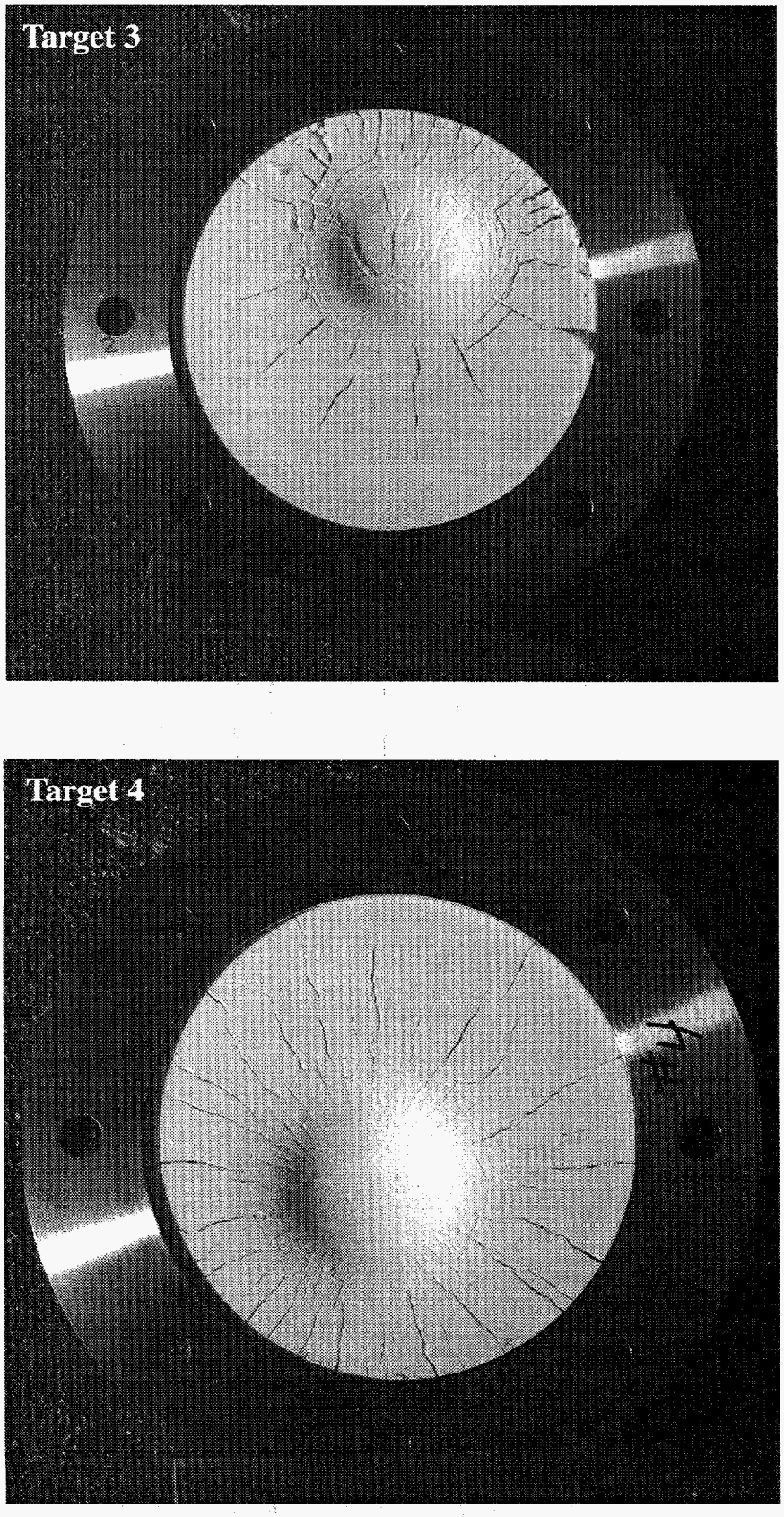

Figure 16: PBX 9501 targets 3 (top) and 4 (bottom) showing circumferential and radial cracking due to projectile impact.

Figure 17: PBX 9501 targets 6 (top) and 8 (bottom) showing circumferential and radial cracking due to impact.

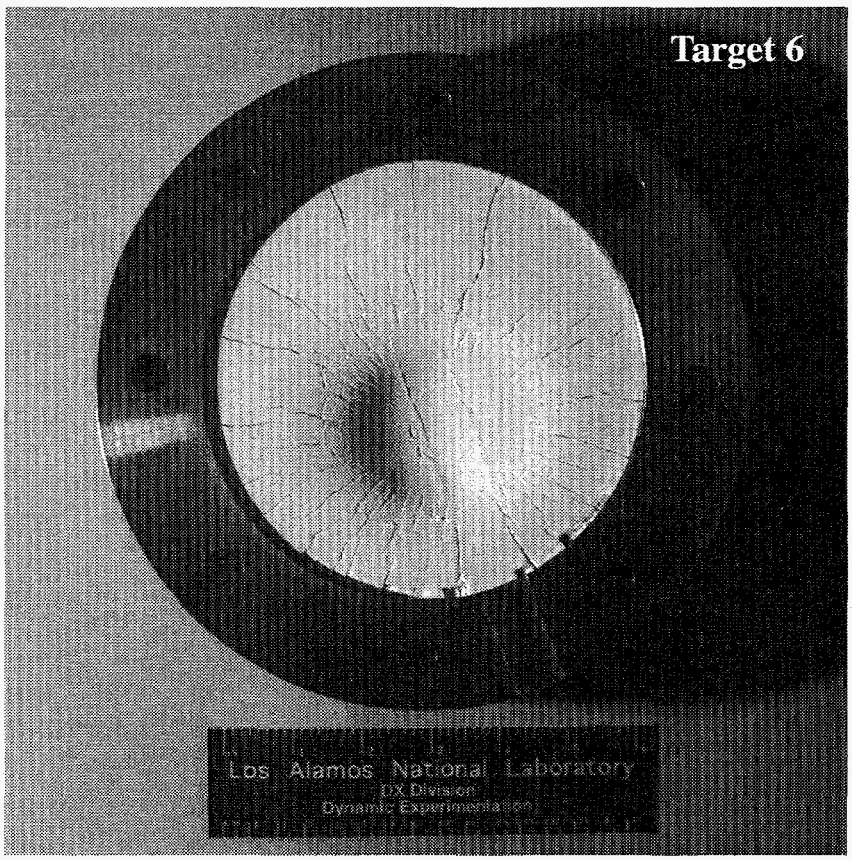

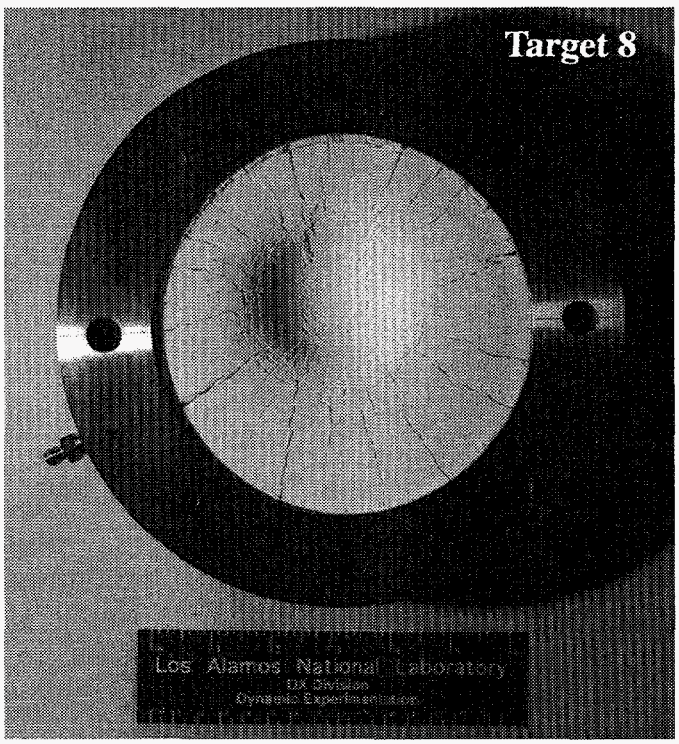

Core samples have been taken of regions C, M, and R from targets 4, 6, and 8. Immersion densities of the solid pieces are given in Table 6 and should be compared to the average initial density of 1.837 (g/cm^3). For each target, Region C has the lowest density and Region R has the highest density. This supports the notion that material is forced from the center to the edges. Chip samples from each coring have been submitted for chemical and thermal analyses. A piece of material from Region D of target 8 has been evaluated using Scanning Electron Microscopy (SEM). Each of 5 surfaces (two machined surfaces, three crack surfaces) is shown in Figures 18 and 19.

Target test 9, at 246.3 ft/s, produced a semi-violent reaction in that it blew away the cover plate, but did not cause serious damage to the rest of the target like the higher velocity experiments did. Also, not all of the HE was consumed, and small pieces were recovered from the firing mound. Some of these pieces have been examined under light microscopy and some under SEM. A light microscope picture of one of these pieces is presented in Figure 20 and shows an unusually high degree of permanent, mechanical twinning in the HMX. This indicates that of these crystals experienced very high levels of stress. Twinning is not evident in some of the HMX crystals taken from an undamaged portion of target 1, and there are fewer twin planes in each crystal that do exhibit this phenomenon. A picture of unformulated, coarse HMX crystals is given for comparison (no twinning), also in Figure 20.

SEM photomicrographs of HE material from target test 9 are given in Figure 21. Three pieces were examined; each appeared to show a different level of HMX reaction: rubblized crystals without reaction, partial reaction as evidenced by the presence of some crystalline matter in a matrix of "foam," and material that appears to have been nearly all melted with some release of decomposition gases. An image of coarse HMX powder at approximately the same magnification is provided for comparison. (The HMX in PBX 9501 is 71.25 wt % coarse grade.)

Table 6. Density of PBX 9501 core samples (g/cm^3), post test.

Sample Region	Target 4	Target 6	Target 8
C	1.754	1.734	1.735
M	1.760	1.756	1.766
R	1.793	1.798	1.786

PBX 9501 Machined Surfaces. Target #8.

Figure 18: Machined surfaces of PBX 9501, from target test 8, post test.

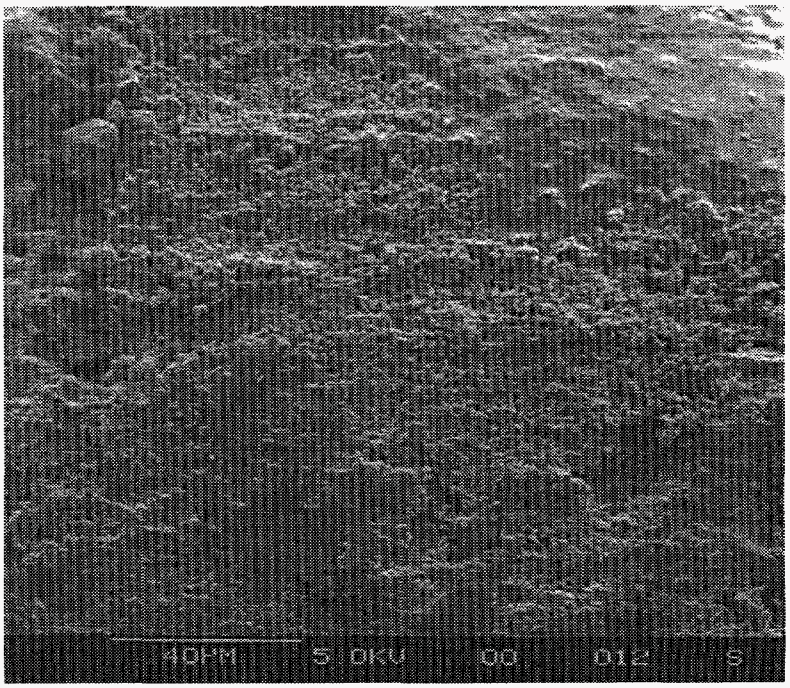

A) Contacting sylgard layer (600x mag.)

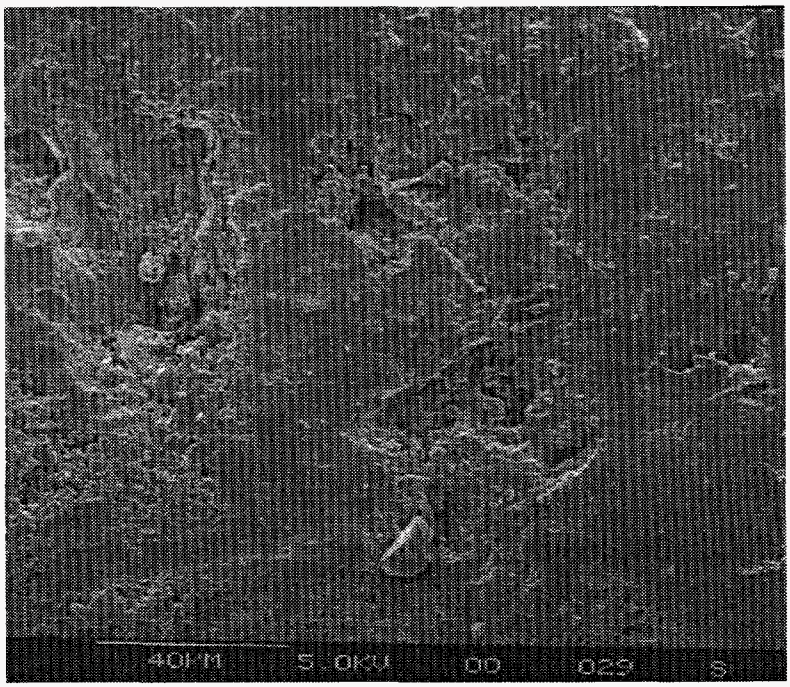

B) Contacting holder wall (600x mag.)

Figure 19: Fracture surfaces of PBX 9501, from target test 8, post test.

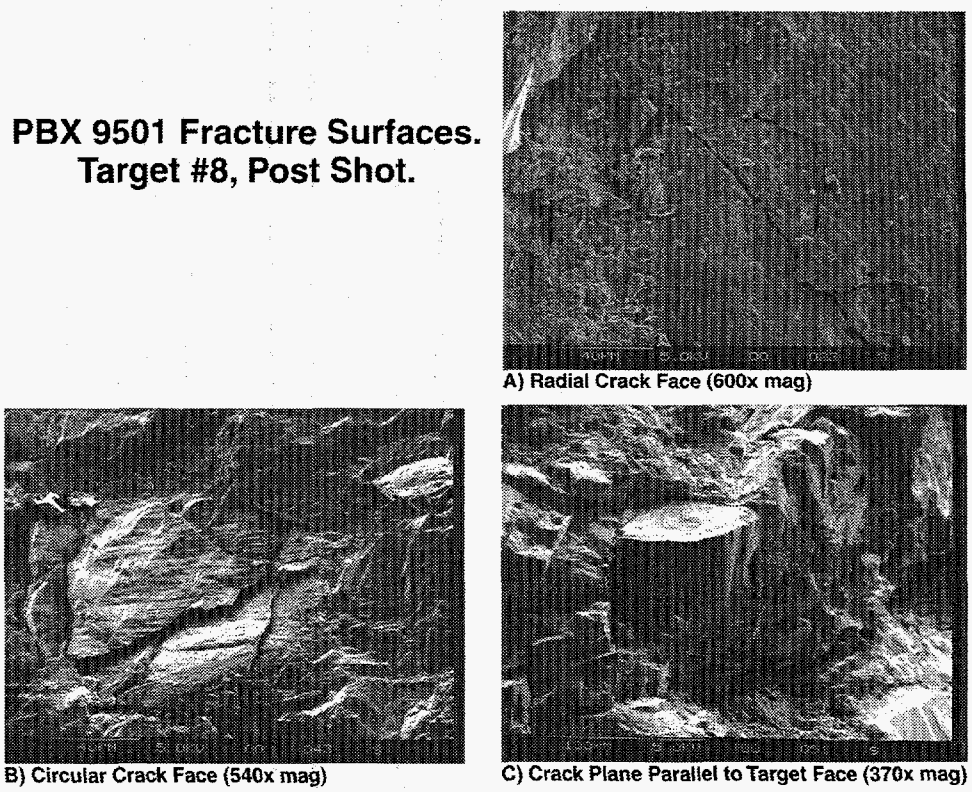

Figure 20: Light microscope images of A) Coarse HMX powder, B)The micron scale of the images, C) Sample of PBX 9501 from target 1 D) The sample of PBX 9501 from target 9, which shows evidence of twinning in the HMX crystal.

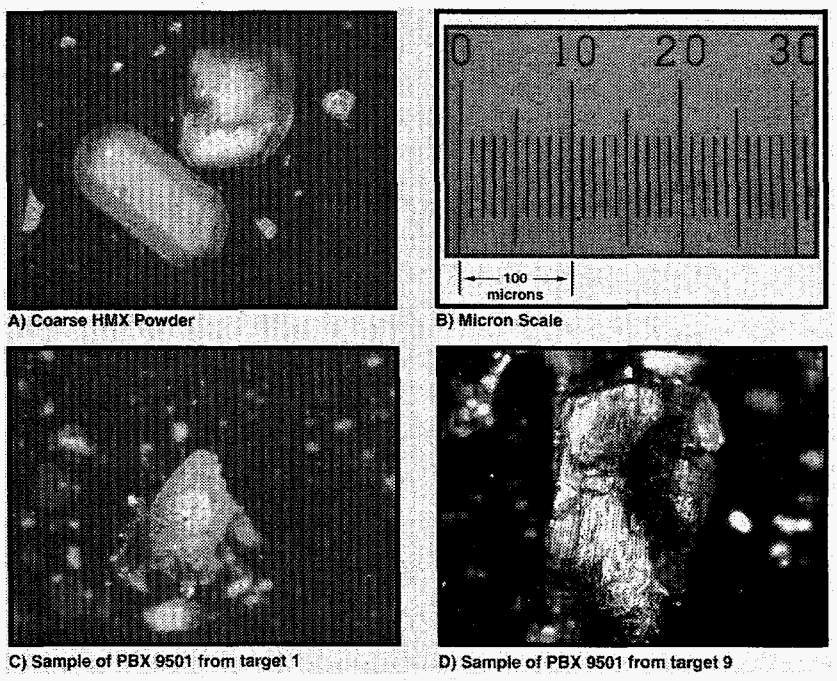

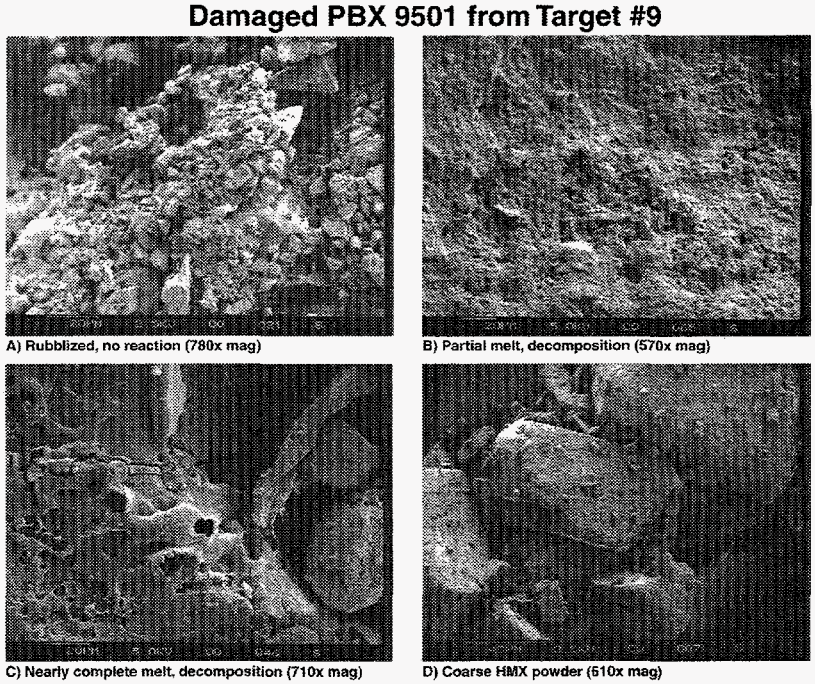

Figure 21: PBX 9501, recovered from semi-violent reaction of target test 9.

V. MODELING PROBLEM SET-UP

A. Approach

The primary objectives of the modeling effort were to support the design and analysis of the experiments, to develop an analytical model for PBX 9501, and to develop an ignition criterion for PBX 9501. The code selected to perform the analysis was DYNA2D, a nonlinear, explicit, two-dimensional, finite element code developed by LLNL. The code does not include explosive reaction or chemistry models.

The mesh used in the calculations is reproduced in Figure 22. A sample distorted mesh after the projectile has rebounded is shown in Figure 23 (215 ft/s, target 4). The material properties for the calculations were derived using a combination of data from the literature and the selected data from the experiments. The material properties and the use of the experimental data will be discussed in Section VI.

B. Ignition Criterion

A low level reaction, or ignition, criterion for PBX 9501 has been proposed by Richard Browning.[6] It is expressed in the following equation:

$$R = K \bullet P^{2/3} \bullet (MaximumShearStrainRate)^{1.27} \bullet t^{1/4}$$

In this power law criterion, the parameter K is a characteristic constant to be determined, P is the pressure and t is the time. The explosive will begin to react violently at a level below full detonation when the value R exceeds some predetermined value. To support development of the model the ORION post processor for DYNA2D was modified to generate contour plots based on this expression.

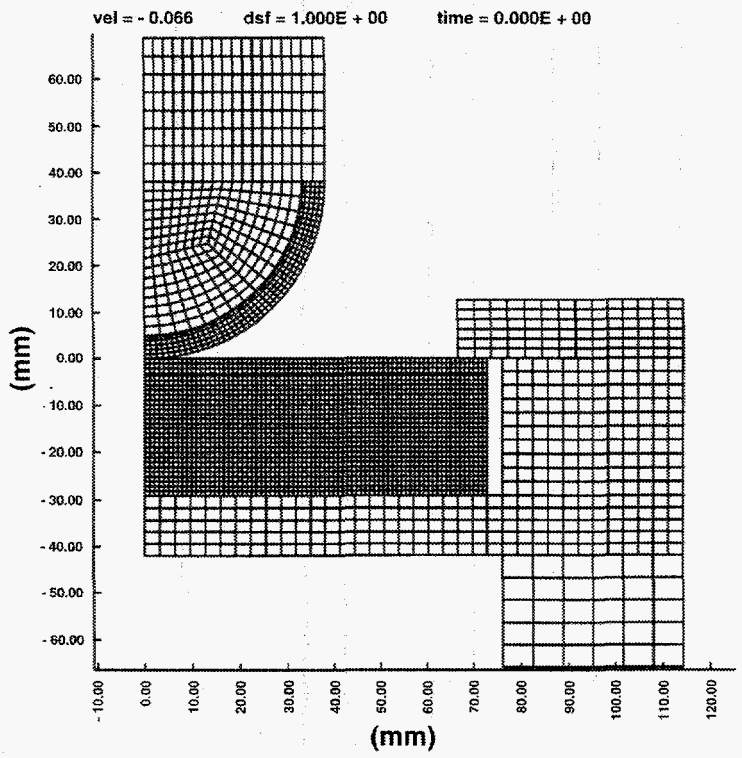

Figure 22: DYNA2D mesh used to model spigot gun projectile impact on PBX 9501 target.

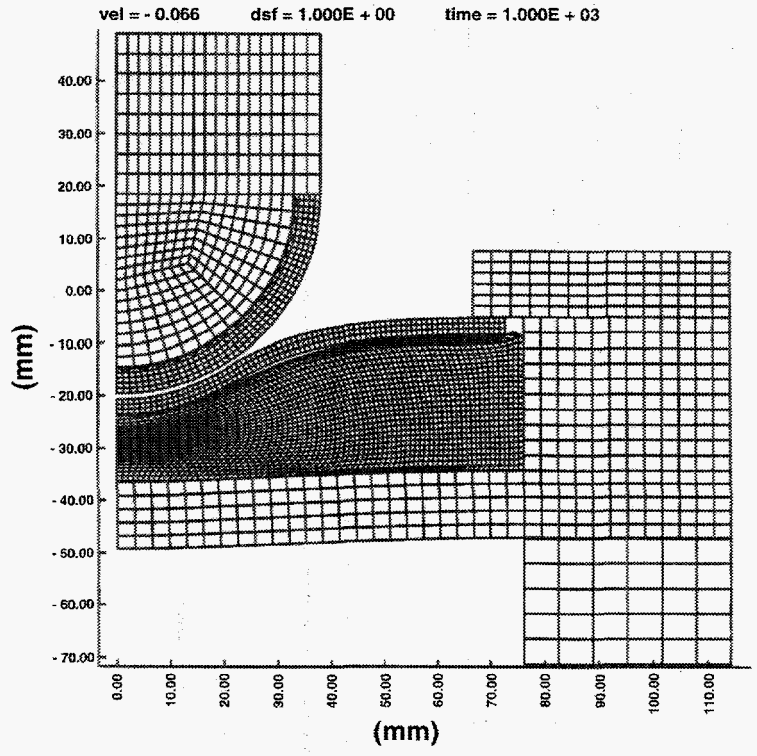

Figure 23: Distorted DYNA2D mesh for target test 4 (DF15-2330)

VI. MODELING ANALYSIS AND RESULTS

A. Material Properties and Calibration

Finding adequate material properties for PBX 9501 became even more difficult when examination of the initial no-go experiments revealed that the explosive underwent extensive fracture and deformation. Radial and circumferential cracks were visible in the recovered unreacted targets, and the explosive had expanded to fill the annular gap. This means that the fracture response of PBX 9501 is an important contributor to the overall mechanical response of the explosive, at least in this geometry. However, there is little or no PBX 9501 fracture data available.

The lack of fracture data, coupled with the importance of the fracture response, led us to use the front surface dent and rear surface deformation data from the unreacted no-go experiments to calibrate the material properties. Table 5 summarizes the live target experiment matrix and lists the measured dent and deformation data. For the initial modeling analyses presented in this paper, the dent in the steel cover plate was defined as the difference between the deepest part of the dent and the average depth at 40 mm from this point. The deformation of the target's rear surface was defined as the maximum deformation of the rear surface referenced to the edge of the holder.

It was necessary to adjust both the 304 ss and the PBX 9501 parameters to achieve good agreement with the measured deformation measurements. Although 304 ss is reasonably well characterized, there is a range of properties available in the literature. The "calibrated" stress strain curve developed for 304 ss is plotted along with several alternative curves in Figure 24. The calibrated material properties used in the calculations are listed in Table 7. It is important to note that the calibrated material properties are within the scatter of the available data.

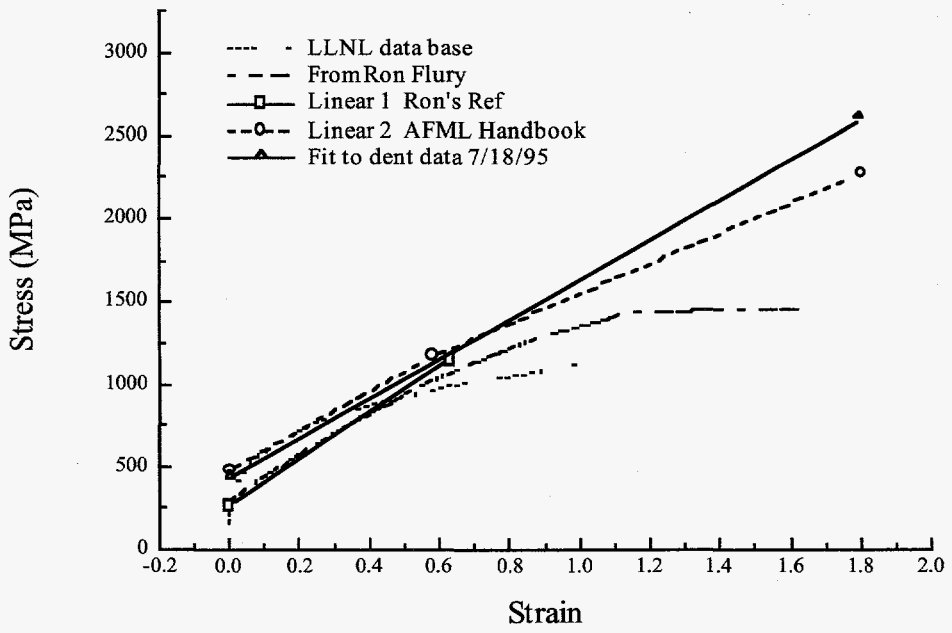

Figure 24: Stress-strain data for 304 stainless steel (304ss).

Table 7: Material properties used in DYNA2D calculations.

	304 Stainless Steel (304 ss)	PBX 9501	Sylgard 184
DYNA2D Material Model	10/4 E-P Hyd	10/4 E-P Hyd	7 Rubber
Density (g/cm^3)	7.850	1.828	1.394
Shear Mod (MPa)	$7.7x10^{4}$ (1)	$2.69x10^{3}$ (1)	800
Yield (MPa)	440(2)	8	--
Plastic Mod	1200(2)	800(2)	--
DYNA2D Spall Model	--	2	--
Spall P_c (MPa)	--	-30(2)	--
c_0 (mm/μs)	4.7	2.683	--
S_1	1.5	1.906	--
Γ	1.5	1.5	--

(1) Shear calculated using Flury's Youngs Modulus and Possion Ratio.
(2) Adjusted to fit dent data.

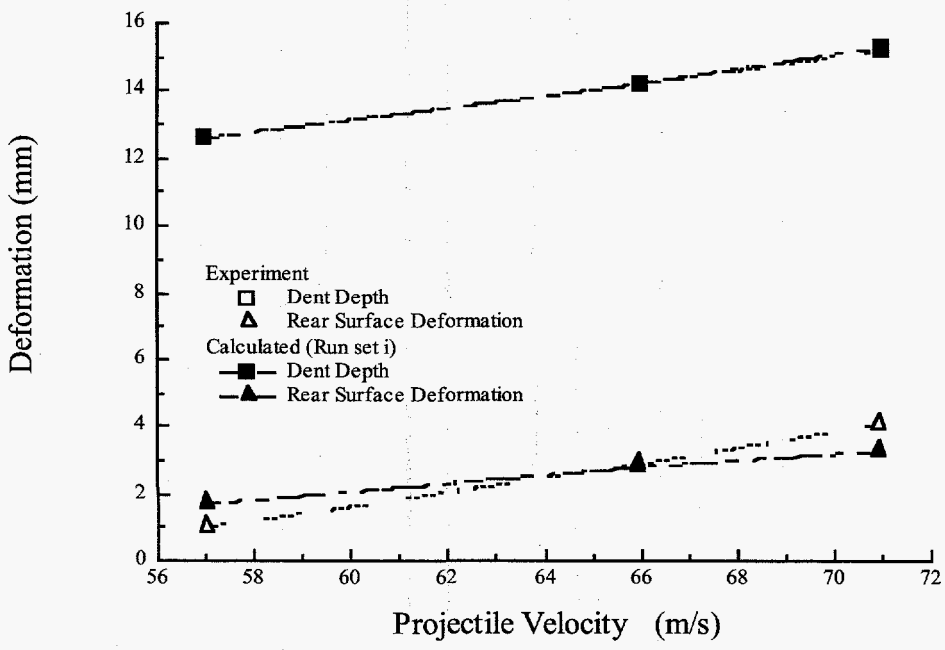

Figure 25: Comparison of calculated and measured front dent depth and rear surface deformation.

All of the calibration adjustments were accomplished using the 214.9 ft/s test data (target 4). The calculations at the other velocities were accomplished after the final set of parameters was chosen. The results are presented in Figure 25. The calculated front surface dent depths overlay the measured dent data. The calculations did not do quite as well with the rear surface deformation. The present set of properties should be considered as preliminary, and additional work on the material parameters will be accomplished as the program progresses and more data become available. It is important to keep in mind that other combinations of material properties may work as well if not better. Also a two-dimensional code cannot deal adequately with the radial cracks observed in the experiments; the calibrated fracture model is only an approximation at best.

Using the experimental data to derive the material properties in this manner allowed us to proceed with analysis of the experiments and develop the ignition criterion with some confidence in the code predictions. This approach essentially bypasses the problem, for the time being, posed by the lack of traditional published material properties. One of the goals of the program is the continuing development of material model parameters for PBX 9501.

The linear dependence of both the front and rear surface deformation upon projectile velocity is interesting. Also the lack of scatter in the deformation data indicates that the projectile velocity measurements are highly repeatable.

B. Calculations

The material property models discussed above were used to generate analytical modeling predictions to compare with the active measurements. Because DYNA2D does not contain reactive chemistry models, the comparisons are only valid up to the time the explosive starts to react. Because the start of reaction can cause only small increases in temperature and pressure, depending on how fast the reaction grows, it is difficult to identify with the experimental measurements. When comparing calculations with gauge output, it is generally assumed that the pinducer is responding to the stress and not the pressure. However, many of the calculated plots include both stress and pressure profiles in both the PBX 9501 and the steel. The sign convention in DYNA2D has pressure positive in compression, while stress is negative in compression. In order to compare these variables and the measurements, stress was plotted as positive in compression.

The calculations were run with two-dimensional symmetry that necessarily assumes that the projectile hits the center of the target. As noted above and documented in Table 5, this was not normally the case. Since the projectile could not be moved off-center in the calculation, the comparisons were made by editing at a distance from the center equivalent to the distance between the actual impact point and the gauge location. No attempt has been made to estimate the effect of the non-symmetrical impact on the calculated response. Figure 26 demonstrates how the calculated axial stress at the rear surface of the PBX 9501 changes as a function of the radial displacement from the center line.

C. Carbon Foil Gauges

The results from the carbon film gauges potted in the Sylgard layer were disappointing but probably not surprising. The gauge was intended to measure the pressure-time profile at the front surface of the PBX 9501. The gauges did provide the shock arrival time and a short portion of the initial pressure buildup before the trace went negative in a very nonphysical way. They did not provide much support for the analytical effort. The early time carbon foil gauge data are compared with DYNA2D calculations in Figure 27 and Figure 28.

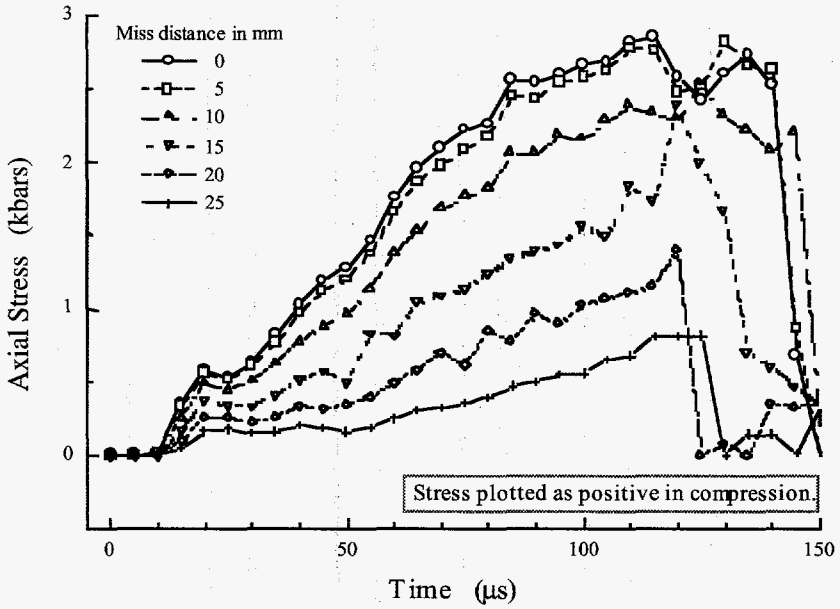

Figure 26: Axial stress at the rear surface of the PBX 9501 as a function of radial offset from the centerline, target test 5 (DF15-2347).

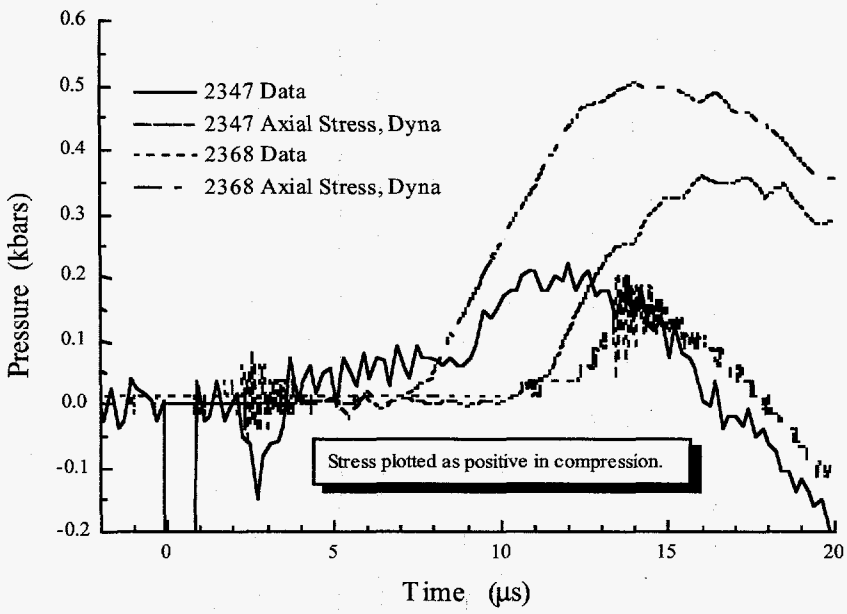

Figure 27: Carbon foil guage data and calculations, target test 5 (DF15-2347) and 6 (DF15-2368).

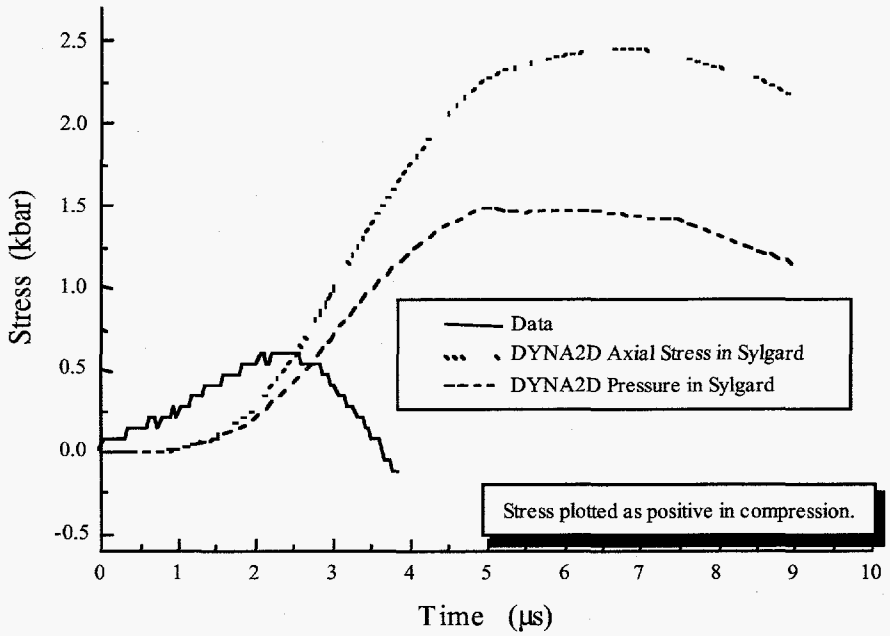

Figure 28: Carbon foil guage data and calculations, target test 10 (K3-1304).

D. Radial Pinducers

One of the reasons for fielding pinducers with a radial orientation was to measure the time at which the solid explosive came in contact with the holder wall. This information would provide a useful check on the PBX 9501 material model and, in particular, the fracture model. No correlation between the data and the analytical model analysis was evident in any of the radial pinducer traces. In particular, there was no correlation with the predicted pressure in the explosive at the time of impact with the side wall and the pinducer traces. A review of one calculation did show some correlation of the data trace structure with the calculated arrival of stress and strain fields, which were generated by the overall deformation of the steel holder. This might indicate that the gauge, as installed, was adversely affected by these fields and that the stress/strain fields in the holder swamped the signal generated by the explosive coming in contact with the side wall. It is also quite possible that the contact of the explosive with the side wall did not create a stress pulse as large as predicted and was too small to pick out of the background noise. A comparison of calculated values with the data from a radial pinducer is presented in Figure 29. The calculation predicts that the explosive would impact the side wall at about 340 μs.

As stated previously, the radial pinducers on live targets tests 9 and 10 were positioned in contact with the explosive rather than flush with the inside wall of the holder. Again there was no correlation between the calculated radial stress, or pressure, in the explosive and the pinducer measurement. It is not clear what to expect from this geometry at early times.

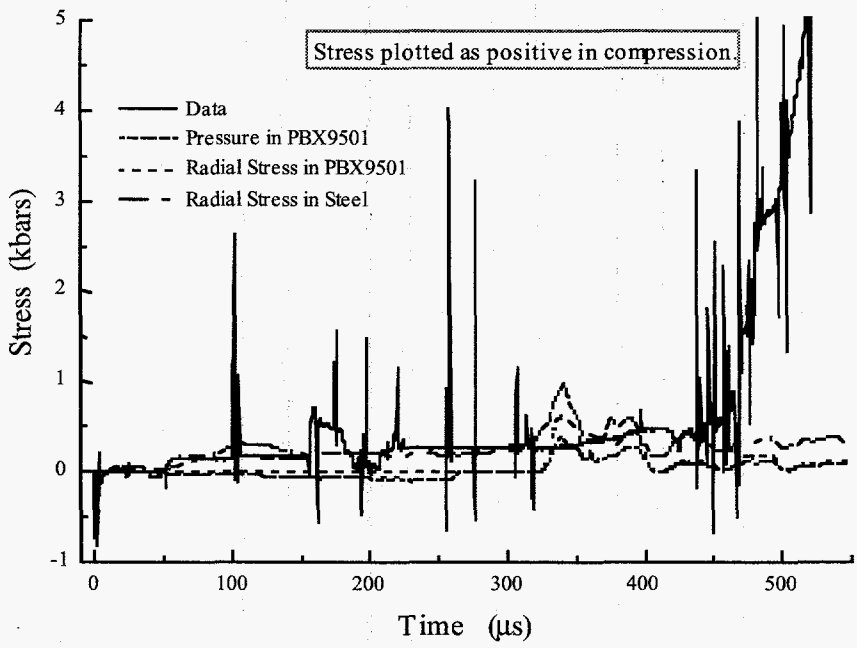

Figure 29:Target test 4 (DF15-2330), radial pinducer 4, experimental and calculated data.

E. Rear Surface Pinducers

The rear surface pinducers provided early time data that, at least initially, looked to be quite useful. There is some encouraging correlation between the measurements and the calculation for the gauges closest to the point of impact. The gauges further from the impact point generally measured only very low pressure levels at early time as expected. However, analysis of the calculations versus data correlation was complicated by the temperature sensitivity of the pinducer. As discussed in Section IV, the pinducer gauge output drops with increasing temperature. Unfortunately, there are a number of temperature sources in these experiments. These include friction as the explosive slides across the surface of the holder, shock compression and deformation of the explosive and, of course, energy released when the explosive starts to react. The combination of temperature and pressure sensitivity makes the early time data difficult to interpret. Temperature sensitivity is a problem common to most pressure transducers, and a solution is not immediately obvious.

Figures 30 to 35 present comparisons of the DYNA2D calculations with the pinducer data. Usually only the pinducer closest to the point of impact is included. Because of the difficulty in separating the effects of temperature response from pressure response, no detailed review of the data/analysis correlation will be presented with the exception of a few general comments.

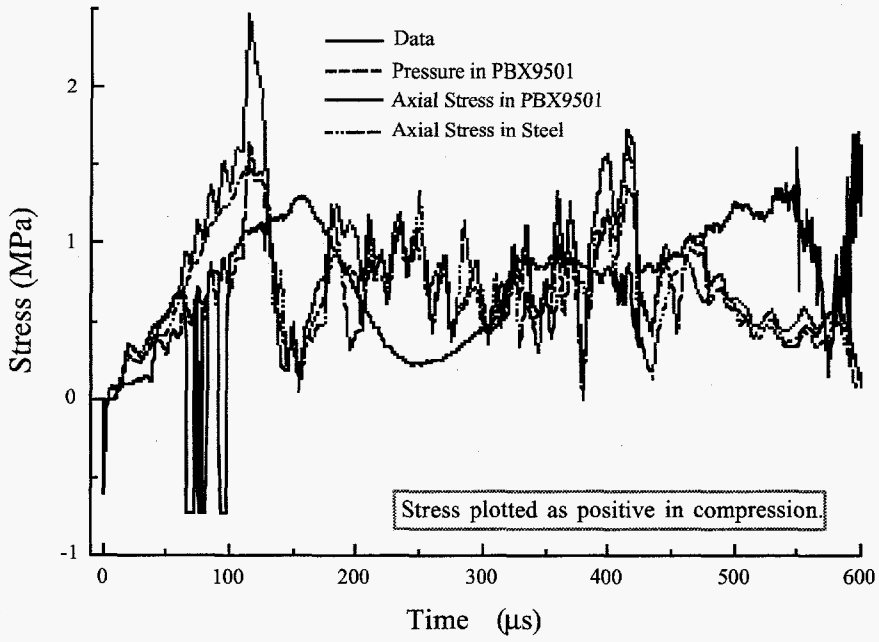

Figure 30: Target test 5 (DF15-2347), pinducer 2, experimental and calculated data.

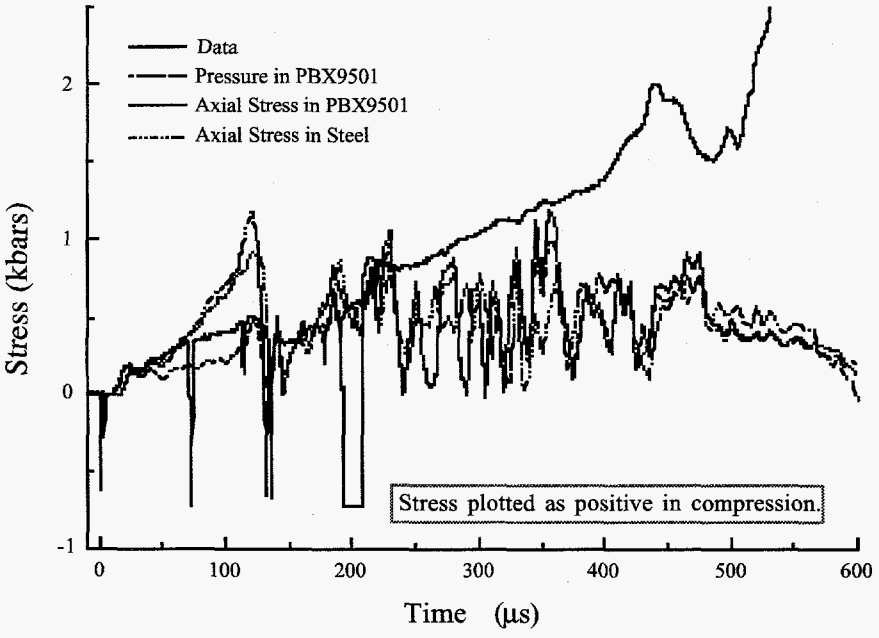

Figure 31: Target test 5 (DF15-2347), pinducer 3, experimental and calculated data.

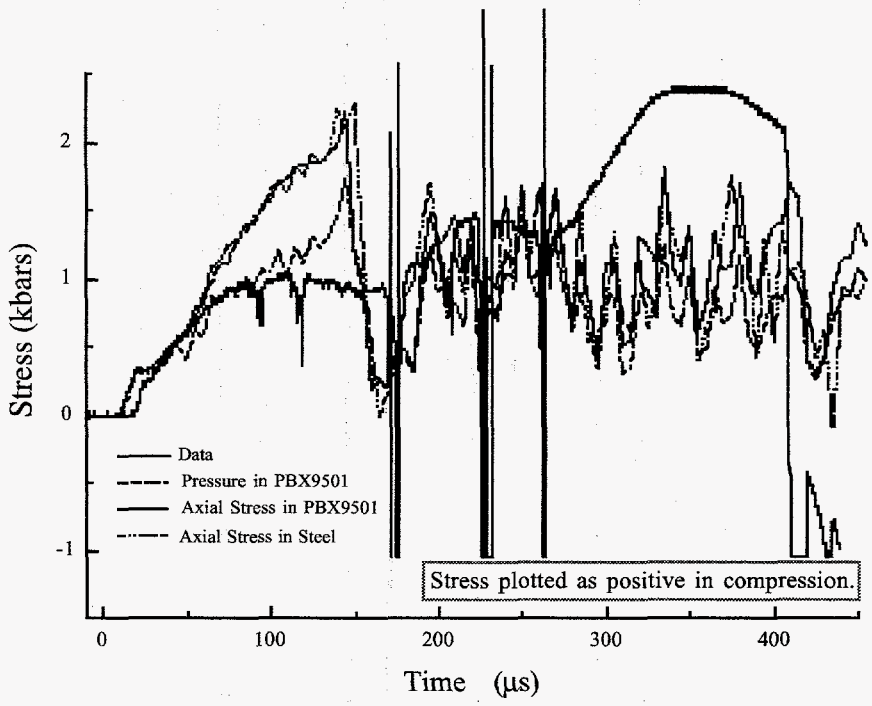

Figure 32: Target test 6 (DF15-2368), pinducer 2, experimental and calculated data.

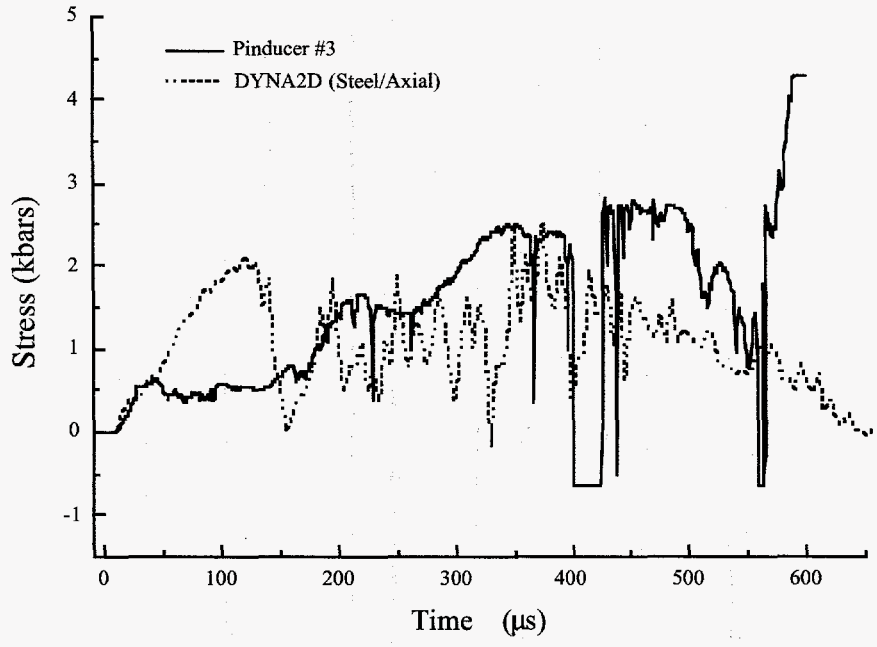

Figure 33: Target test 7 (K3-1235), pinducer 3, experimental and calculated data.

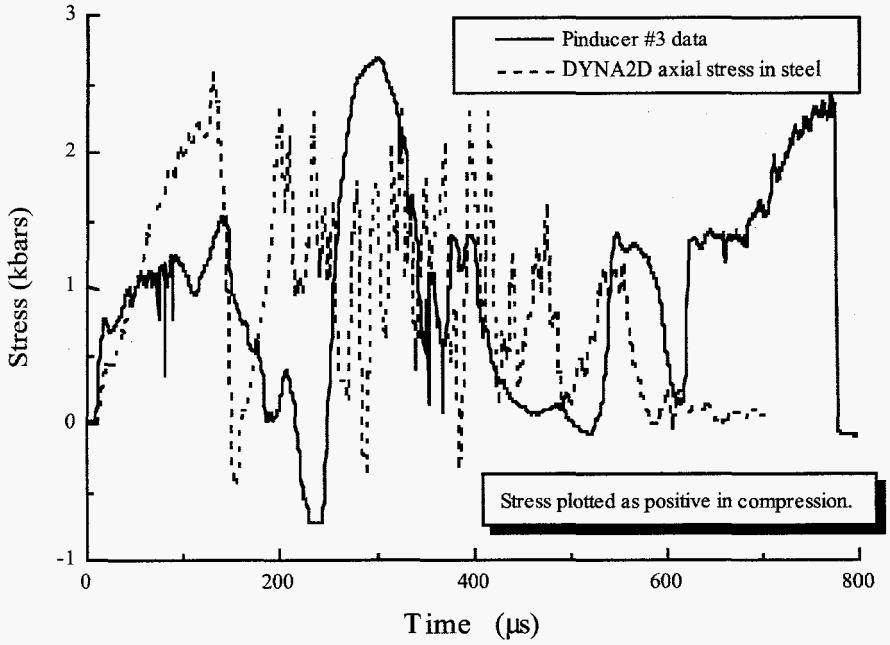

Figure 34: Target test 9 (K3-1290), pinducer 3, experimental and calculated data.

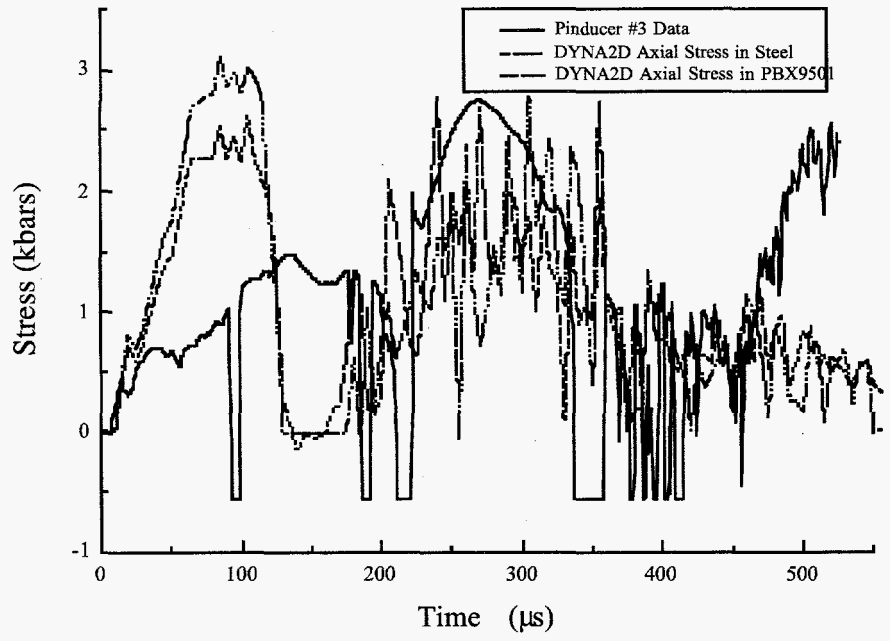

Figure 35: Target test 10 (K3-1304), pinducer 3, experimental and calculated data.

The calculations always overpredict the stress in the 100 μs time regime, about the length of time that DYNA2D predicts that the material starts to fracture. From a modeling point of view this could indicate that the material model is too stiff or that the fracture strength is too high. However, the decrease, or leveling out, of the gauge output could also be due to a change in temperature as discussed above. There is no way to know which, if either, is correct. However, given the number of heat generating sources in the experiment, there is a surprising amount of correlation at later time for several of the measurements.

This serves to emphasize a basic problem with the present experiments as they relate to model development. Reliable and accurate pressure measurements are necessary to develop material models and an ignition criterion. However, the spherical projectile, combined with the large amount of fracture and the relatively long time-to-ignition, result in conditions where accurate pre-ignition pressure measurements are extremely difficult, if not impossible. To acquire the information necessary for model development, it may be necessary to pursue new innovative measurement techniques and/or experiments designed specifically to measure material properties.

F. Ignition Criterion

Initial application of the power law criterion to the threshold experimental data generated values of R that increased with impact velocity. This allowed selection of a trial threshold value for R. Experimental threshold data for a different geometry (e.g., modified projectile radii or mass) are required to determine if this value will work for other geometries or if additional parameter adjustment is required. Figure 36 presents the predicted threshold velocities for two other projectile diameters based on the trial calibration.

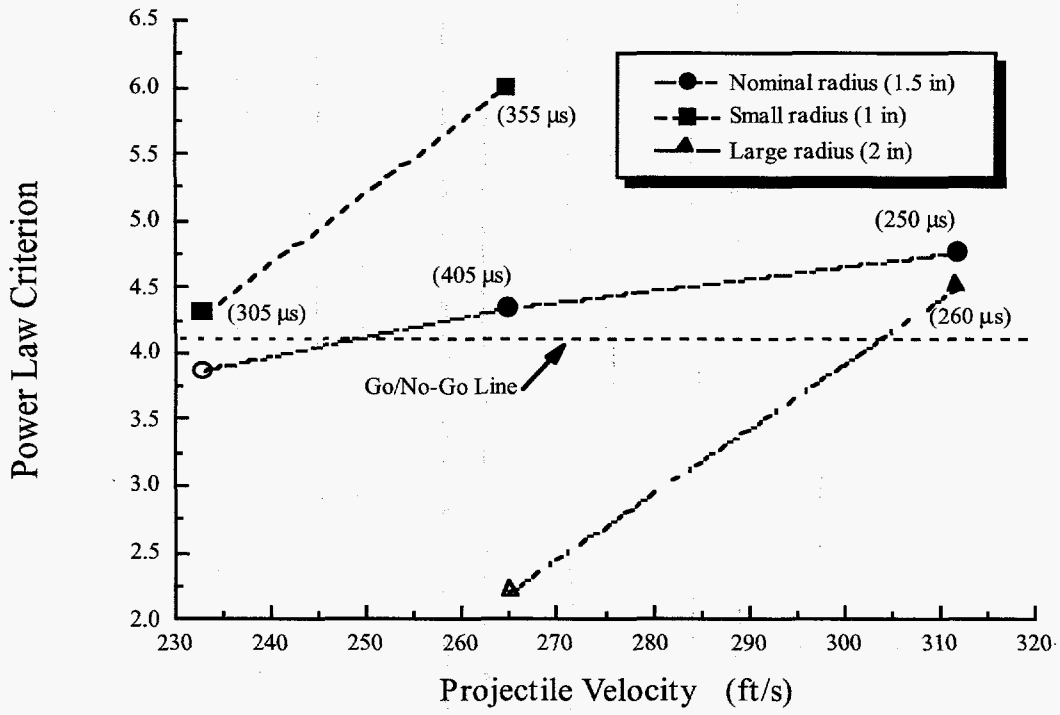

Figure 36: Power law criterion predictions for various projectile radii.

As implemented, the power law ignition criterion assumes a uniform pressure-time load profile in the explosive. The expression is not integrated, or summed, over time. The large amount of fracture that occurs in the PBX 9501 prior to ignition invalidates that assumption in the present experiments. The calculated pressure as a function of time, at the point where the power law criterion reached the maximum value for target test 5 is plotted in Figure 37. The pressure departs from a smooth curve as soon as the material starts to fracture. The implementation of the ignition model in the code needs to be revised to accommodate this sort of response.

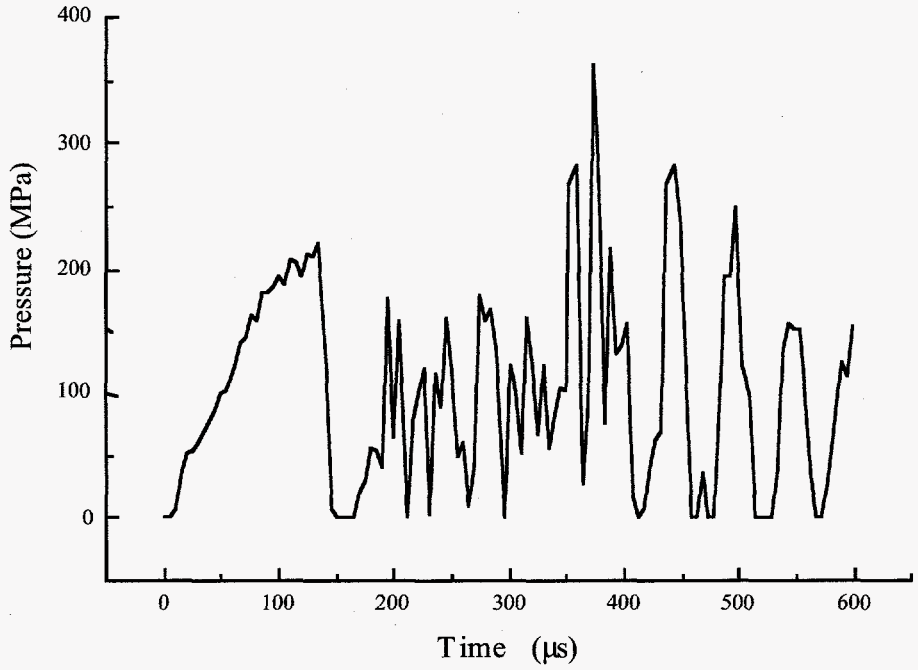

Figure 37: Calculated pressure at ignition criterion, worst-case location, target test 5 (DF15-2347).

VII. EXPERIMENTAL AND MODELING CONCLUSIONS

A. Experimental

Several basic conclusions can be drawn from the experimental effort.

1. PBX 9501 can produce violent reactions or partial detonations at impact velocities well below that required for the shock-to-detonation transition (SDT). The pressure gauge data indicate we are not seeing a fully developed detonation; however, the energy release would be sufficient to cause severe damage and dispersal of heavy metals if such an event occurred to a nuclear weapon. It is highly improbable because of the slow speed at which the reaction progresses that even the worst case scenario could produce any nuclear yield for this particular initiation process. However, at this point we cannot draw similar conclusions about other initiation processes such as multiple impacts, e.g. double bullet or sequential fragment impact.
2. Impact generated compression, fracture, and shear flow produce significant heat with very little delay. After this, however, it takes 0.5 to 1.0 ms for the reaction to build to its violent climax.

3. Compared to the typical small scale Taylor test, this particular target/test system shows remarkable consistency and a very sharp velocity threshold transition at or near 246 ft/s. Although the gauge data are noisy, they show a consistent progression of reaction severity as the impact velocity is increased.
4. Although the data are by no means conclusive, they indicate that reaction does not begin at a single well-defined point and spread from there, but rather heating and possibly burning starts over a large area and may sensitize a large portion of the volume of damaged HE. After this system heats up for up to 1 ms, at least one reactive wave is somehow generated and moves across much of the mass of material at velocities of 1 to 2 mm/μs. Thus, the wave is probably locally subsonic and does not have a well defined front.

B. Modeling

The modeling effort supporting the experiments can be summarized as follows:

1. An initial analytical model for PBX 9501 has been developed for DYNA2D using the dent and deformation data from the unreacted experiments and available data from the literature.
2. The relatively long time-to-ignition, coupled with the large amount of material deformation prior to ignition, makes it extremely difficult to make the accurate and reliable early time pressure measurements required for analytical model development. The overall question of material model requirements, measurements, and experimental design to support such measurements needs to be carefully examined.
3. An initial calibration of a proposed PBX 9501 power law ignition criterion has been accomplished. Additional experiments with modified geometries (e.g., different projectile diameters or mass) are needed to ascertain if this criterion calibration will work for other geometries or if additional model development is needed. The implementation of the ignition model in the DYNA2D codes needs to be refined to deal with the problems introduced by the large amount of target deformation and fracture.

VIII. FUTURE OBJECTIVES

A. Experimental

It would be good to confirm that heating and reaction begin over a large area. We have considered several ways of evaluating this. We have plans to design and fabricate several targets with thick glass backs and will attempt to photograph light emission from reacting areas as a function of time with a fast framing camera. We have also considered making some targets with an array of ionization pins through the back of the target. Many of the pins would be biased with a constant resistance so that the local conductivity could be measured as a function of time. This could be used to indicate reaction and flow in the region of the pin. Finally, we are considering making some targets with heat sensitive film imbedded in the HE and between the HE and the metal surfaces of the target. Unfortunately, this will change the frictional forces and may significantly alter the velocity threshold and the ignition processes involved.

B. Modeling

There is a wide range of objectives for future analytical modeling efforts that build upon the present work. These include the following:

1. Continue to provide analytical support for experiment and target design as well as analysis of the results.
2. Continue to improve material models based on existing and new information.
3. Perform experiments using modified geometries to investigate the preliminary ignition criterion cali-

bration under simple changes in geometry and generally support ignition criterion development.
4. Work toward experiment/instrumentation designs that would provide reliable data to support material model development and verification.
5. Perform detailed examination of PBX 9501 samples from the highest velocity no-go target.

Longer term objectives include the following:
1. Once an ignition criterion is developed, test its portability by installing and testing it in the ABAQUS finite element program.
2. Perform experiments on LX-10 as a cross check with the Chidester experiments.
3. Perform experiments on other explosives of interest.

IX. ACKNOWLEDGMENTS

We gratefully acknowledge the programmatic support of the project leader Phil Howe and the program manager George Hurley. We also would like to acknowledge the technical contributions and helpful suggestions of Ron Flury and Richard Browning, both of ESA Division, for the successful conception, initiation, and continuation of this project. The project results reported here have been a culmination of numerous and sundry efforts throughout ESA, MST, and DX Divisions, without whom this work would have not been possible. Accordingly, we would like to also acknowledge the following individuals and their contributions to the project:

ESA DIVISION

Roger Osantowski and the TA-16-410 Assembly Technicians
Responsible for assembly of the first ten PBX 9501 targets.
Clinton Shonrock, ESA-DE
Responsible for initial target designs and assembly drawings.

MST DIVISION

Rusty Gray, MST-5
Responsible for coordinating ferrite scope measurements and analysis of targets 3and 5 hardware.
Mike F. Lopez, MST-5
Responsible for obtaining ferrite scope measurements on targets 3 and 5 hardware.
Karl Staudhammer, MST-5
Responsible for low strain rate ferrite scope measurements on 304 ss used for comparison purposes.

DX DIVISION

Access Control Office, DX-4, Janette Lujan and Joseph Lopez
Responsible for the execution of coordination and safety of firing site activities in area K-1.
Rudy Archuleta, DX-4
Responsible for HE inventory and firing site support at Kappa Site, TA-36.
Bob Critchfield, DX-4
Responsible for photodiode velocity screen box design and development, firing site work.
Rodger Hall, DX-7
Responsible for new design and testing of photodiode trigger screen.
George Harper, DX-5

Responsible for HE coring and machining of damaged PBX 9501 targets.

Aaron Honey, DX-2

Responsible for digital image production for view graphs and reports.

Leo Martinez, DX-5

Responsible for initial 0.5-in. bore gun drawings and designs.

Don Murk, DX-4

Responsible for all TA-40-15, DF Site firing site work and early development work.

Mike Osborn, DX-5

Responsible for interfacing with the JCT/NTS shop personnel on tracking machine parts and completion, and responsible for gun barrel strain gauge electronics package.

Kathy Pfeufer, DX-5

Responsible for high pressure gun designs and some of the target and projectile designs.

Walter Quintana, DX-4

Responsible for powder loading most of the cartridges.

Lori Rohlev, DX-7

Responsible for new design and testing of photodiode trigger screen.

Victor Sandoval, DX-4

Responsible for firing site support at Kappa Site, TA-36.

Larry Smith, DX.-5

Responsible for initial target designs, modified drawings for original 0.75-in bore gun

Ken Uher, DX-2

Responsible for foil gauge design and production, PFN board production, initial work on photodiode trigger screen, and graphite rod trigger screen.

Eddie Viramontes, DX-4

Responsible for TA-36-3, Eenie Site firing site preparation and work, and responsible for pneumatic firing system design for spigot gun.

JCI/NTS shop

Responsible for mechanical fabrication and repairs of all hardware for the targets,0.75-in. bore guns, high pressure guns, and 0. 75-in. spigots and firing mechanism.

REFERENCES

1. Gibbs, T. R. and Popolato, A. "LASL Explosives Property Data," University of California Press, Los Angeles, CA (1980).
2. Chidester, S. K., Green, L. G., and Lee, C. G. "A Frictional Work Predictive Method for the Initiation of Solid Explosives from Low Pressure Impacts," Tenth (Int). Det. Symp., Office of Naval Research, 786 (1993).
3. Dobratz, B. M., "LLNL Explosives Handbook: Properties of Chemical Explosives and Explosive Simulants," UCRL-52997, University of California Press, Livermore, CA (1981).
4. Los Alamos National Laboratory, "PBX 9501 Target Assembly," Drawing No. 139Y-11-60005 (April 1994).
5. Lucht, R. A. and Charest, J. A., "Calibration and Use of a Rugged New Piezoresistive Pressure Transducer," Shock Compression of Condensed Matter–1995, Proc. Conf. APS Top. Grp., Seattle, WA, p. 1041 (1995).
6. Richard V. Browning, ESA-EA, personal communication, January 1995.

Distribution List

DX-Division Office	DX-DO	MS P915
S. G. Bardenhagen	ESA-EA	MS P946
R. V. Browning	ESA-EA	MS P946
G. A. Buntain	DX-2	MS C920
R. R. Critchfield	DX-4	MS P952
S. Chidester	LLNL	MS L282, LLNL, Livermore, CA
J. K. Dienes	T-14	MS B214
E. N. Ferm	DX-3	MS P940
R. L. Flury	ESA-EA	MS P946
B. F. Henson	CST-6	MS J567
P. M. Howe	DX-DO	MS P915
R. Henninger	XHM	MS F663
G. F. Hurley	PDNW	MS F630
D. J. Idar	DX-2	MS C920
E. S. Idar	XNH	MS F664
R. A. Lucht	DX-1	MS P950
J. Maienschein	LLNL	MS L282, LLNL, Livermore, CA
J. Middleditch	CIC-19	MS B256
R. J. Scammon	ESA-EA	MS P946
C. B. Skidmore	DX-2	MS C920
J. B. Snow	DX-2	MS C920
J. R. Stine	DX-2	MS C920
J. W. Straight	DX-5	MS P942
K. J. Uher	DX-2	MS C920